Phytomedicine 100 (2022) 154069

Contents lists available at ScienceDirect

Phytomedicine

journal homepage: www.elsevier.com/locate/phymed

Original Article

Metabolomics based mechanistic insights to vasorelaxant and cardioprotective effect of ethanolic extract of *Citrullus lanatus* (Thunb.) Matsum. & Nakai. seeds in isoproterenol induced myocardial infraction

Fatima Saqib [a], Muqeet Wahid [a], Arwa Abdulkreem AL-Huqail [b,*], Hanadi Talal Ahmedah [c], Nicusor Bigiu [d,*], Marius Irimie [d], Marius Moga [d], Romina Alina Marc (Vlaic) [e,*], Oana Lelia Pop [f], Liana Maria Chicea [g]

[a] Department of Pharmacology, Faculty of Pharmacy, Bahauddin Zakariya University, Multan, Pakistan
[b] Department of Biology, College of Science, Princess Nourah bint Abdulrahman University, P.O. Box 84428, Riyadh 11671, Saudi Arabia
[c] Department of Medical Laboratory Technology, Faculty of Applied Medical Sciences, King Abdulaziz University, Rabigh 25732, Saudi Arabia
[d] Faculty of Medicine, Transilvania University of Brasov, 500019 Brasov
[e] Food Engineering Department, Faculty of Food Science and Technology, University of Agricultural Sciences and Veterinary Medicine, 400372 Cluj-Napoca, Romania
[f] Department of Food Science, University of Agricultural Science and Veterinary Medicine, 400372 Cluj-Napoca, Romania
[g] Faculty of Medicine, "Lucian Blaga" University of Sibiu,Romania

ARTICLE INFO

Keywords:
LC-ESI MS/MS
Cardiac hypertrophy
Cardioprotective
Citrullus lanatus
Metabolomics

ABSTRACT

Background: Cardiovascular diseases (CVDs) are a significant cause of morbidity and death in the current world, posing a challenge to both developing and industrialized nation's health systems. *Citrullus lanatus* (Thunb.) Matsum. & Nakai. seeds have long been utilized to supplement and enhance health and treat cardiovascular illnesses. However, its treatments for CVDs are still unknown. More research is required to fully comprehend the impact of *C. lanatus* seeds on vasorelaxation and myocardial infractions.
Purpose: Therefore, an integrated metabolomics profiling technique was used to investigate possible pathways of *C. lanatus* in isoproterenol (ISO)-induced myocardial infarction (MI). Isoproterenol causes long-term cardiac hypertrophy by causing cardiomyocyte compensatory loss, eventually leading to heart failure.
Methods: In vitro models of vasoconstriction, atrium, and *in vivo* models of invasive blood pressure measurement and isoproterenol (ISO) induced cardiac hypertrophy in rats were used to understand underlying mechanistic by LC-MS/MS based dynamic metabolomics analysis of the serum and heart samples to be investigated the effect of ethanolic extract of *C. lanatus* (Cl.EtOH).
Results: Cl.EtOH exhibited vasorelaxant, negative chronotropic, and inotropic effects in *in-vitro* models whereas, a potent hypotensive effect was observed in normotensive rats. The Cl.EtOH protected the animals from ISO-induced myocardial infarction (MI) with therapeutic interventions in left ventricular thickness, cardiomyocyte hypertrophy, mRNA gene expression, biochemical assays, and metabolomic profiling of serum and heart tissues.
Conclusions: For the first time, our study confirmed that C. lanatus seeds (Cl.EtOH) possess significant antihypertensive and prevent ISO-induced myocardial infarction. These findings comprehensively demonstrated mechanistic insights of Cl.EtOH in vasorelaxation and myocardial infarction. The current study provides evidence for further mechanistic studies and the development of C. lanatus seeds as a potential therapeutic intervention for patients with cardiovascular disorders.

Abbreviations: ACN, Acetonitrile; CCB, Calcium channel blocker; CH, Cardiac hypertrophy; Cl.EtOH, Hydroethanolic extract of C. lanatus seeds; eNOS3, Endothelial nitric oxide synthase 3; FA, formic acid; Log (pKi), Logarithmic of predicated Inhibition Constant (pKi); MeOH, Methanol; MI, Myocardial infarction; MMP9, Matrix metallopeptidase 9; MM-GBSA, Molecular mechanics energies combined generalized born and surface area; TFA, trifluoroacetic acid; VGCC, Voltage-gated calcium channel β2a..

* Correspondence author.
E-mail addresses: aalhuqail@pnu.edu.sa (A.A. AL-Huqail), nicusorbagiu@unitbv.ro (N. Bigiu), romina.vlaic@usamvcluj.ro (R.A. Marc (Vlaic)).

https://doi.org/10.1016/j.phymed.2022.154069
Received 6 November 2021; Received in revised form 14 February 2022; Accepted 19 March 2022
Available online 25 March 2022
0944-7113/© 2022 The Author(s). Published by Elsevier GmbH. This is an open access article under the CC BY-NC-ND license (http://creativecommons.org/licenses/by-nc-nd/4.0/).

Introduction

Myocardial infarction (MI) is a prominent global cause of death. MI is induced by cardiac hypertrophy characterized by irreversible heart tissue damage (Guo et al., 2016) due to insufficient blood supply, decreasing oxygen supply in heart tissue (Li et al., 2014). An abnormal thickening of the left heart ventricle (LHV) wall reduces left ventricular capacity. Long-term hypertrophy causes cardiomyocyte loss, heart failure, angina, and arterial atherosclerosis (Lee et al., 2017). Research is being conducted globally to discover interventions to protect the myocardium tissues from MI. Prevalent therapies have severe side effects with prolonged dependence on such therapies (Pasupathy et al., 2017). Alternative remedies are being used to overcome these complications, as these are considered safe, effective, and economical (Shaito et al., 2020).

Citrullus lanatus (Thunb.) Matsum. & Nakai., commonly known as Tarbooz (Khare, 2007) (*Cucurbitaceae*), is widely cultivated as edible fruit globally (Koocheki et al., 2007; Renner and Pandey, 2013; Siddiqui et al., 2018). The fruit is eaten raw and roasted besides desserts, salad, snacks, watermelon cake, lemonade, and watermelon rind pickles (Erhirhie and Ekene, 2014; Siddiqui et al., 2018). Drinks and juices made from fruits and seeds are used for freshness, chilling, and thirst-quenching in summer (Rahman et al., 2013). Its seeds, commonly known as *Tukhm-e-Tarbooz*, are used against urinary complaints, hepatic congestion, intestinal catarrh, and gastrointestinal disorders (Khare, 2007). The traditional herbal practitioners use seeds to cure gastrointestinal disorders, urinary disorders, aphrodisiac (Duke, 2008; Perkins-Veazie et al., 2007), cardiovascular disorders, hypotensive (Erhirhie and Ekene, 2014; Rimando and Perkins-Veazie, 2005), and reduce fever (Taiwo et al., 2009). The seeds and fruit have analgesic, anti-inflammatory (Iswariya and Uma, 2017), diuretic, anti-urolithiatic (Siddiqui et al., 2018), antioxidant (Gill et al., 2011), hypotensive, cardioprotective (Massa et al., 2016), and antiulcerative activities (Gill et al., 2011).

C. lanatus seed comprises 32 - 40% oil content with a higher proportion of polyunsaturated fatty acid (Raihana et al., 2015). Mabaleha et al., (2007) and Taiwo et al., (2009) reported that *C. lanatus* seeds are rich in linoleic acid, approximately 54 - 68.6%. *C. lanatus* seed also contains oleic acid (13 - 16%), stearic acid (5 - 7%), palmitic acid (9 - 12%) with smaller quantities of myristic acid (0.04%), palmitoleic acid (0.07%), margaric acid (0.1%), linolenic acid (0.3%) and arachidic acid (0.29%) (Ouassor et al., 2020; Raihana et al., 2015; Taiwo et al., 2009). Besides fatty acid, phytosterols (471.5 mg/100 g) are present in *C. lanatus* seed oil, including sitosterol (55 mg), stigmasterol (5 mg), and stigmastadienol (31 mg) (Ouassor et al., 2020). Abu-Reidah et al., (2013) reported polar fraction of *C. lanatus* fruit and seed is richer in polyphenols and other polar phytoconstituents. *C. lanatus* polar fraction contains L-citrulline, protocatechuic acid 3-glucoside, rutin, calodendroside A, orientin, Isovitexin, ajugol, and quercitrin. (Abu-Reidah et al., 2013; Siddiqui et al., 2018)

Despite traditional uses of seeds of *Citrullus lanatus* (Thunb.) Matsum. & Nakai. In cardiovascular ailments, no previous study exits rationalizing its folk medicinal usage. The present work used *in vitro, in vivo,* and molecular docking models to investigate the cardioprotective properties and metabolomics insights of *Citrullus lanatus* (Thunb.) Matsum. & Nakai. seeds (Cl.EtOH). The ISO induced-MI model was used to clarify the potential mechanisms of Cl.EtOH is based on heart and serum metabolomics and gene expressions.

Materials and Methods

Preparation of Extract

From May to July 2018, *C. lanatus* seeds were obtained from fresh fruits pulp farmed in local farms in Multan, Punjab, Pakistan, rendering them free of fruit pulp. A taxonomist Dr. Zafarullah Zafar, from Institute of Pure and Applied Biology, Bahauddin Zakariya University Multan, Pakistan, identified (herbarium voucher number: P.K.F. 1916/30) the seeds and fruit of C. lanatus. A plant specimen was submitted in the same institute's Herbarium with P.K.F. 1916/30) voucher.

After removing the husks from the seed, the interior section was crushed into coarse seeds powder using an herbal grinder. The pulverized material (120 g) was hot macerated in the Soxhlet apparatus with hydroethanol (70% ethanol and 30% aqueous). It evaporated under reduced pressure at 36 ± 2 °C in a rotary evaporator (Buchi R-200) to get a thick brownish yellowish tinted extract (Cl.EtOH) with a yield of 45%. The Cl.EtOH solution was kept at -20 °C in an amber container. On the day of the experiment, the Cl.EtOH was diluted to the appropriate concentration in distilled water or normal saline.

Chemicals and materials

Analytical grade solvents methanol, trifluoroacetic acid (TFA), ethanol, acetonitrile (ACN), and formic acid (FA) were procured from Sigma Aldrich Chemicals Co. USA. All chemicals for buffer solutions, analytical grade standards for HPLC and experiments were procured from Merck and Sigma Aldrich Chemicals, Co. USA. N(ω)-nitro-L-arginine methyl ester, Isoproterenol (ISO), and RIPA Buffer was procured from Sigma Aldrich Chemicals, Co. USA. The primary rat antibodies (ANP, IL-6, eNOS3, β-actin) and rabbit anti-horseradish peroxidase (HRP) antibodies were procured from Cambridge, UK. Angiotensin II, cyclic guanosine monophosphate (cGMP) level, and nitrate/nitrite (NO) immunoassay kits were procured from MyBioSource Inc. California, United States. All serum commercially available biochemical kits were purchased from Abcam (Cambridge, UK), MyBioSource (California, USA), and Sigma Aldrich Chemicals (USA).

Sample Preparation for HPLC and LC-ESI- MS/MS

Cl.EtOH was diluted in 1 ml 100% methanol for HPLC and LC-ESI-MS/MS analysis, and the supernatant was collected after centrifugation for 12 min at 14000 rpm. The supernatant was filtered using a 0.22 μm syringe filter.

LC ESI-MS/MS analysis

LC ESI-MS/MS (LTQ XL mass spectrometer, Thermo Electron Corporation, Waltham, MA, USA) was used to analyze Cl.EtOH to conduct a preliminary screening of bioactive compounds. (Seraglio et al., 2016; Wahid et al., 2021). The direct injection of sample into an electron spray ionization (ESI) probe conFig.d to both positive (M+) and negative (M-) ionization modes and a mobile phase comprised solvent A: 0.1% FA in methanol (MeOH) and Solvent B: 0.1% FA in aqueous and acetonitrile (ACN) (80:20) were used for separating compounds. The optimal chromatographic parameters for separation were; mobile phase flow rate (0.4 ml/min), the column temperature (25 °C), sample injection volume (8 μl), mass-spectrum range (50 - 1000 m/z), and column size (C-18, 2.1 mm × 100 mm, 3 μm). The mobile phase gradient was adjusted for solvent A (v/v) as follows: 98%, 98 - 80%, 80 - 70% 70 - 10% and 10 - 98% from 0 - 4.0 min, 4.0 – 8.0 min, 8.0 – 15.0 min, 15.0 – 17.0 min, and 17.0 – 20.0 min, respectively. The ideal ion source settings for mass spectrometric analysis were; ion spray voltage for positive mode: 5500 V, ion spray voltage for negative mode: -5500 V; curtain gas (CUR): 25 psi; nebulizer gas (GS1): 55 psi; auxiliary gas (GS2): 55 psi; ion source temperature: 400 °C. As a CUR and GS2, nitrogen was employed. Ions are isolated in an ion trap and fragmented using collision-induced dissociation (CID) energies ranging from 10 to 45, depending on the stability of the parent precursor ions used in tandem mass spectrometry. Thermo Scientific's X-Calibur 3.0 (Waltham, MA, USA) was used to gather and process ESI-MS/MS data.

Identification of compounds

The bioactive constituents were identified by comparing their mass spectra chromatogram to previously published data and reference libraries, including the Mass Bank of North America (Mo-NA; http://mona.fiehnlab.ucdavis.edu, Accessed on June 18, 2021) and the European Mass Bank (https://massbank.eu/MassBank/, Accessed on June 18, 2021). The spectra of compounds were compared to high-resolution masses and MS/MS fragmentation of libraries and databases (Syed et al., 2021). ChemDraw 18.0 (PerkinElmer informatics, Waltham, MA, USA) was used to elucidate the structure

Quantification of bioactive compounds by using analytical HPLC-DAD UV/Vis

HPLC method optimization

Cl.EtOH was processed to RP-HPLC (Agilent Technologies, Germany) to validate and quantify the bioactive compounds (β – sitosterol, epigallocatechin, chlorogenic acid, gallic acid, ellagic acid, vanillin, vitexin and, kaempferol) (Qamar et al., 2021; Wahid et al., 2021). The sample was analyzed in RP-HPLC using a C-18 column (C18, 4.6mm × 150 mm, 5 μm), and the following chromatographic parameters were optimized; mobile phase, column temperature, injection volume, flow rate, and detection wavelengths. The mobile phase comprises Solvent A: 0.1% TFA in MeOH, and Solvent B: 0.1% TFA in Aqueous and ACN (80:20) was used to visualize peaks. The optimal chromatographic conditions were; temperature (25 °C), mobile phase flow rate (0.8 ml/min), column sample injection volume (8μl), and optimal detection wavelengths (250, 270, 280, and 320 λ). The mobile phase gradient was adjusted for solvent A (v/v) as follows: 95%, 95 - 90%, 90 - 80% 80 - 10% and 10 - 95% from 0 - 4.0 min, 4.0 – 8.0 mins, 8.0 – 14.0 min, 14.0 – 20.0 min, and 20.0 – 30.0 min, respectively. The results were compared with UV spectra and external standards' retention time (Rt).

Validation of the analytical method

The validation method was determined under prescribed guidelines of the International Conference on Harmonization (ICH) and described in our previous report (Qamar et al., 2021).

Preparation of external standards: A stock solution of external standards (β - sitosterol, epigallocatechin, chlorogenic acid, gallic acid, ellagic acid, vanillin, vitexin, kaempferol) dissolved in 1 ml 100% methanol at concentration 150 μg/ml, and the supernatant was collected after centrifugation for 10 min at 14000 rpm; stored at -20 °C. On the analysis day, the stock solution was diluted to further 100 μg/ml and 50 μg/ml. The supernatant was collected and filtered using a 0.22 μm syringe filter.

Linearity, limits of detection, and quantification: For linearity validation, dilutions (7.81 - 500 μg/ml) of external standards were prepared to assess the linearity detector response by constructing a standard curve based on the concentration and the peak area of each standard. The detection limits (LOD) and quantification limits (LOQ) were calculated using the formula below.

$$LOD = 3.3\sigma \div S$$

$$LOQ = 10\sigma \div S$$

where σ is the intercept standard deviation and S is the slope of the linear regression equation.

Specificity: A total volume of 8 μl of extracts and external standards samples were injected in RP-HPLC under the optimal chromatographic parameters mentioned above. The chromatographic peaks and retention time (Rt) of extracts and external standards were compared to determine peak purity. The calibration curves for each external standard were used to quantify the peaks.

Precision and repeatability: The precision and repeatability of the current method for each external standard were studied on interday (n = 4) and intraday (n = 4 on three consecutive days) under the optimal chromatographic parameters mentioned above, and the relative standard deviation (RSD) were determined.

Accuracy and recovery: The accuracy and recovery of the current method for each external standard were determined by retrieving external standards from Cl.EtOH. Three different strengths of external standards (50 μg/ml, 100 μg/ml, and 150 μg/ml) were used for this method: 50 μg, 100 μg, 150 μg of external standards, and 100 mg of Cl. EtOH samples were mixed to get a final concentration of external standards; 50 μg/ml, 100 μg/ml, and 150 μg/ml. A total volume of 8 μl mixture sample was injected in RP-HPLC under the optimal chromatographic parameters mentioned above. The sample recovery percentage of an external standard was estimated using the following equation.

$$\%Recovery = (observedconcentration \div actualconcentration) \times 100$$

Animals and housing conditions

The protocols were approved by the Department of Pharmacology ethical committee (vide No. EC /04-PhDL/S2018), and the studies strongly aligned with the Commission of Laboratory Animal Resources (Rowan, 1979). Sprague-Dawley rats (170 ± 20 g) and mice (28 ± 3 g) were obtained without discrimination of gender for experimental purposes from the same faculty. The animals were housed in the animal house that followed a dark/light cycle with standard food and free access to tap water under controlled circumstances (22 ± 4 °C). Rats and mice were killed through cervical dislocation.

Ethics Statement

ARRIVE guidelines, UK Animals (Scientific Procedures) Act 1986 and accompanying recommendations, EU Directive 2010/63/EU for animal research or National Institutes of Health guidance (NIH Publications No. 8023, revised 1978) for the care and use of laboratory animals were followed in all experiments. The Bahauddin Zakariya University Ethical Committee (EC /04PhDL-S2018) approved the study dated (EC /04PhDL-S2018) dated 26th March 2018.

Isolated tissue experimentation

The methodology described by Saqib and Janbaz (2016) and Gilani et al., (2008) was used for *in vitro* studies.

Isolated aorta preparation

The thoracic aorta was dissected from rats following cervical dislocation and immersed in Kreb's solution aerated with carbogen. All adhesive fatty tissues were removed carefully without damaging the aortic endothelium lining. Each aortic ring (2 - 3 mm) preparation was fixed in a 15 ml tissue organ bath that had been previously filled with the Kreb's solution accreted with carbogen and maintained at 37 °C using a circulating thermoregulator. Before testing the drug, a preloaded force of 2 ± 0.1 g was applied to aortic rings preparation and was allowed to equilibrate for 50 ± 5 min with buffer drainage with new Kreb's solution; after 8 ± 2 min. A force-displacement transducer (Model FORT100) was used to record the physiological response of the tissue. Signals were amplified through Power Lab® (4/25) and displayed in Lab Chart Pro (Version 7). The physiological activity was assessed immediately before the test drug dose and was estimated as a percent contraction. The test or drug materials were sequentially administered after equilibration.

This study was used to evaluate the cholinergic and nitric oxide (NO), based endothelium-derived relaxing factor (EDRF), intact

endothelium, and denuded endothelium aortic preparations. For denuded endothelium aortic preparation, intima of aorta ring was rubbed with curved forceps. The presence or absence of endothelium function was confirmed by relaxation of phenylephrine (1 μM) induced contraction with acetylcholine bolus administration (1 μM), 70 - 80% relaxation in contraction confirmed the presence of endothelium function (intact endothelium). In contrast, further increases in contractions confirmed the absence of endothelium function (denuded endothelium) (Kamkaew et al., 2011). K^+ (80 mM), phenylephrine (1 μM), and K^+ (25 mM)) induced contractions on both aortic preparations in a tissue organ bath were used to investigate the putative vasorelaxant activity of Cl. EtOH.

Preparation of isolated paired atria

The heart was dissected from rats following cervical dislocation and immersed in Kreb's solution aerated with carbogen. Ventricles and all adhesive fatty tissues were removed carefully without damaging the pacemaker, and atria preparation was fixed in a 15 ml tissue organ bath that had been previously filled with the Kreb's solution accreted with carbogen and maintained at 37 °C using a circulating thermoregulator. Before testing the drug, a preloaded force of 1 ± 0.1 g was applied to aortic rings preparation and was allowed to equilibrate for 30 ± 5 min with buffer drainage with new Kreb's solution; after 8 ± 2 min. A force-displacement transducer (Model FORT100) was used to record the physiological response of the tissue. Signals were amplified through Power Lab® (4/25) and displayed in Lab Chart Pro (Version 7). The physiological activity was assessed immediately before the test drug dose and was estimated as a percent contraction. The test or drug materials were sequentially administered after equilibration.

In vivo experimentation

Evaluation of maximum tolerated dose

The maximum tolerable extract dosage was studied in six groups of rats. Normal saline and five doses of the extract were given orally every day for 28 days at 50, 100, 150, 200, and 300 mg/kg. The body weight, behavioral changes, clinical indications of distress, and death of animals were followed for 28 days. (Elasoru et al., 2021).

Evaluation of blood pressure and hemodynamic parameters in anesthetized rats

Healthy rats (250 - 300 g) were anesthetized with diazepam (i.p. 5 mg/kg) and ketamine (i.p. 85 mg/kg) separately for satisfactory anesthesia without modifying cardiovascular parameters within normotensive limits (Saqib and Janbaz, 2016). Rats were fixed on dissecting table in a supine position, and the temperature was maintained with an overhead lamp. The tracheotomy was performed, and the trachea was cannulated with a polyethylene (18G) tube to ease respiration. The cannulation of the right jugular vein was performed for intravenous injection of Cl.EtOH and drugs, while carotid artery cannulation was performed to record the changes in hemodynamic parameters with a pressure transducer (MLT 0699), filled heparinized saline (50 IU/ml). Signals were amplified through Power Lab® (4/25) and displayed in Lab Chart Pro (Version 7). The exposed region was coated with a wet cotton swab and allowed to equilibrate for 13 ± 5 min before administering any drug. Acetylcholine (Ach; 1 μg/kg) and adrenaline (Adr; 1 μg/kg) was administrated for standard hypotension and hypertensive response prior to testing material.

L-NAME induce acute hypertension

For the acute antihypertensive study, a solution of L-NAME, an nitric oxide synthase inhibitor, was administered intravenously (20 mg/kg) to normotensive Wistar rats. Cl.EtOH was given intravenously twenty minutes after L-NAME injection when maximal elevation in L-NAME-induced blood pressure.

Isoproterenol induced chronic myocardial infarction

According to Eladwy et al., (2018), the study was designed for 21 days to induce MI. Isoproterenol (ISO) and Cl.EtOH was dissolved in normal saline. Forty-two male albino rats (150 - 200 g) were segregated randomly into seven groups and housed in separate cages. Each group contains six animals.

Group I: The negative control group was administered orally normal saline at a dose of 10 ml/kg

Group II: The intoxicated control group was administered ISO subcutaneously at a dose of 5 mg/kg/day for 14 days (from the 8th day of the experiment to the 21st day).

Group III: The standard drug treatment group was administered orally carvedilol at the dose of 10 mg/kg/day for 21 days.

Group IV: The standard drug treatment group was administered orally verapamil at the dose of 10 mg/kg/day for 21 days.

Group V: The extract treatment group was administered orally Cl. EtOH at dose 75 mg/kg/day for 21 days.

Group VI: The extract treatment group was administered orally Cl. EtOH at dose 150 mg/kg/day for 21 days.

Group VII: The extract control group was administered orally Cl. EtOH at dose 150 mg/kg/day for 21 days. The extract control group was used to determine the effects of Cl.EtOH in the absence of ISO on model parameters.

After one hr., pretreatment of carvedilol, verapamil, and Cl.EtOH, subcutaneous injection of ISO (5 mg/kg), was administrated for consecutive 14 days starting from the 8th day until day 21st day, except Group VII, which did not receive the ISO.

Sample collection

After 24 h of last administration of ISO, animals were anesthetized (ketamine i.p. 40 mg/kg), and blood was collected from the retro-orbital sinus to determine biochemical indices in coagulant tubes and anticoagulant tubes containing EDTA. The blood samples were centrifuged at 4500 rpm for 15 min at 4 °C to separate serum and plasma from blood and stored at -20 °C. The animals were slaughtered through cervical dislocation, and heart tissues dissected. Immediately the heart tissues were washed with ice-cold saline and frozen for RT-PCR analysis or preserved in 10% formalin for histopathology studies.

Determination of Biometrical indices

The cardiac hypertrophy was assessed with biometrical indices, i.e., heart weight, heart diameter, left heart ventricular (LHV) weight, LHV thickness, heart weight index (heart weight/body weight ratio), LHV index (left heart ventricular /body weight ratio), tail length index (heart weight/tail length ratio), tibia length index (heart weight/tibia length ratio) (Elasoru et al., 2021).

Histopathological examinations

Hematoxylin and eosin (H&E) staining: The fixed hearts were dehydrated with sequential dilutions of alcohol (70 - 100%), cleaned with xylene, and fixed in paraffin at 56 °C. The heart slices (4 μm thick) were deparaffinized and stained with hematoxylin and eosin (H&E) stains. Digital photos were captured using a 4x and 10x magnification microscope. The total cell count, diameter, and size were measured using ImageJ software (ImageJ, Version 1.44p, NIH, USA).

Masson's trichrome staining: To assess cardiac fibrosis, we used Masson's trichrome staining with certain modifications. The heart slices were incubated for 120 ± 10 min in prewarmed Bouin's solution. The

nuclei were stained for 20 min with Weigert's hematoxylin, while Biebrich scarlet-acid fuchsin solution was used to stain the cytoplasm and muscle for 20 min. The tissue slices were treated with a phosphomolybdic-phosphotungstic acid solution for ten minutes, then a blue aniline solution for 10 min. After 30 s of incubation with 1% acetic acid, the slices were dehydrated with ethanol and xylene. Digital photos were captured using a 4x and 10x magnification microscope. Interstitial and perivascular fibrosis was assessed using ImageJ software (ImageJ, Version 1.44p, NIH, USA)

Determination of serum cardiac biochemical markers

Biochemical indicators for myocardial infarction; alanine transaminase (ALT), lactate dehydrogenase (LDH), creatine kinase MB (CK-MB), creatine kinase (CK), aspartate transaminase (AST), troponin I (cTnI), troponin T (cTnT), angiotensin-converting enzyme (ACE), renin concentrations, brain natriuretic peptide (BNP), arterial natriuretic peptide (ANP), serum interleukin-6 (IL-6), and lipid profiling were determined by commercially available enzymatic kits and quantified by spectrophotometry at 340 nm. Angiotensin II, cyclic guanosine monophosphate (cGMP) level, and nitrate/nitrite (NO) levels were determined by enzyme immunoassays and colorimetric assay kits in accordance with the manufacturer's instructions (Syed et al., 2016).

Quantitative real-time polymerase chain reaction (qRT-PCR)

The frozen heart tissues were homogenized, and total RNA was extracted using TRIzol reagent (Invitrogen) per the manufacturer's instructions. The relative gene expression was determined by RT-PCR using the Bio-Rad CFX96 system. The primers used in this study are IL-6 (F: AGTTGCCTTCTTGGGACTGA R: ACAGTGCATCATCGCTGTTC), arterial natriuretic peptide (F: ATACAGTGCGGTGTCCAACA, R: CGAGAGCACCTCCATCTCTC), cardiac Troponin T (F: CAGAGAGGAGGAAGGTGCTG, R: TTCCCACGAGTTTTGGAGAC), nitric oxide synthase 3 (F: AACTAGACTGGGAGGGAGTCA, R: GGGCAGCAGGATGTCCTAATA), and MMP-9 (F: CCCCCAACCTTTACCAGCTA, R: GGTCAGAACCGACCCTACAA). mRNA expression levels were normalized in a similar sample to housekeeping gene β- actin (F: AGCCATGTACGTAGCCATCC, R: CTCTCAGCTGTGGTGGTGAA).

Western blotting

According to Kumar et al., (2017), proteins were isolated from the left cardiac ventricles. The left ventricle (150 mg) was homogenized in 5 ml RIPA buffer with 1x protease and phosphatase inhibitors (Sigma Aldrich Chemicals, Co., USA) and centrifuged the homogenate at 13,500 rpm for 20 min, then transferred the supernatant to a vial. The Bradford technique was used to determine the protein concentration using standard BSA. Proteins were loaded onto a 10% SDS-polyacrylamide gel electrophoresis (SDS-PAGE) and transferred for 2 h at 110V onto methanol activated 0.2 μm pore size polyvinylidene fluoride (PVDF) membranes (Millipore, USA). PVDF membranes were treated with primary antibodies overnight at 4 °C after being blocked with 5% nonfat milk at room temperature. To eliminate unbound primary antibodies, the membrane was washed three times with 1x Tris-buffered Saline, 0.1% Tween (TBST). The membranes were treated at room temperature for 60 min with a secondary antibody labeled with horseradish peroxidase (HRP, dilution 1:3000). The membrane was then rinsed three times with 1x TBST, and bands were identified using the Gel Doc XR system (Bio-Rad). The research employed rat anti ANP (1:1500 dilution), rat anti IL-6 (1:500 dilution), rat anti eNOS3 (1:1000 dilution), and rat anti-actin (1:1500 dilution). Image J was used to assess the expression of particular proteins, and the results were adjusted to the housekeeping protein β-actin.

Metabolomics Study

The metabolomics investigation was conducted in accordance with Sun et al., (2017) and Wu et al., (2020).

***Sample preparation*:** The LC ESI MS/MS technique was employed for metabolomics, and samples were combined in a 1:1 v/v solution of acetonitrile (ACN) and methanol (MeOH). After thawing the serum samples at 4 °C in an ice bath, 100 μl serum and 400 μl precooled ACN: MeOH were combined and vortexed for 30 - 60 s, sonicated for 10 min at 4 °C, then incubated overnight at -20 °C to precipitate the proteins. Finally, the mixture was centrifuged at a speed of 13000 rpm for 15 min at a temperature of 4 °C; the supernatant was transferred to a dry clean tube and dried. Heart tissues were treated identically, except they were homogenized three times in water (at a 1:10 w/v ratio) using a tissue homogenizer. The dried residues were reconstituted with ACN: MeOH (1:1 v/v), vortexed for 30 - 60 s, sonicated for 10 min, centrifuged at 13000 rpm for 15 min at 4 °C, and then the supernatant was transferred to LC-MS vials.

***Chromatographic conditions*:** Prepared solutions (8 μl) were injected into the LC ESI-MS/MS binary gradient system under chromatographic conditions mentioned in section 2.4, and using mobile phase solvent A: 0.1% FA in aqueous and solvent B: 0.1% FA in acetonitrile.

Data processing and biomarker identification

The ESI-MS/MS data acquisition and processing software X-Calibur 3.0 (Thermo Scientific, Waltham, MA, USA). The metabolites identities were confirmed by comparison of MS/MS spectra with online databases searches HMDB (http://www.hmdb.ca, accessed on 3rd July 2021) and Mass bank of North America (https://mona.fiehnlab.ucdavis.edu/, accessed on 3rd July 2021) based on exact mass measurement (mass error < 5 ppm). The data matrix was imported into R studio with MetaboAnalyst for pathway analysis and enrichment analysis.

SIMCA 14.0 (MKS Umetrics) was used to analyze the serum and cardiac LC-MS/MS metabolomic data. Unsupervised principal component analysis (PCA) was performed to identify metabolic patterns and trends. Following that, we used partial least squares discriminant analysis (PLS-DA) and orthogonal projections to latent structures discriminant analysis (OPLS-DA) to assess and differentiate between experimental groups. Additionally, these models were validated using stringent permutation testing. The variable importance (VIP, VIP > 1) and t-test (p0.05) were used to identify potentially biomarker-relevant metabolites.

Molecular docking

The methodology described by Sirous et al., (2019) was used for Molecular docking experiments.

Ligand Preparation: The prominent bioactive compounds in network pharmacology were used as ligands further to investigate binding forces and stability in target proteins. The three-dimensional structures of ligands were obtained from PubChem (https://pubchem.ncbi.nlm.nih.gov, Accessed date: 15th July 2021) in mol2 format and subjected in LigPrep (Maestro v11.8, Schrodinger suite 2018-4) for ligand ionization, minimization, and optimization. OPLS3e force field was applied for energy minimization and optimization of ligands to enhance accuracy and performance of predicting protein-ligand model that provides the lowest energy conformer. Following Epik tool was used for possible protomers, and ionization states were generated at target pH (7.4 ± 2.0). The tautomeric states were generated for each ionized ligand and used the Desalt to retain the ligands with the most significant number of atoms. The stereoizer was used to generate stereoisomers of each ligand and retained stereogenic chirality data from the input file, with a limit of 10 stereoisomers considered per ligand.

Protein Preparation: The three-dimensional crystallized structure of proteins was obtained from RCSB Protein Databank (RCSB PDB)

(https://www.rcsb.org, Accessed date: 28th April 2021) in PDB format and subjected to Protein Preparation module (Maestro v11.8, Schrodinger suite 2018-4) for protein generating het states, hydrogen bond assignment, ionization, minimization, and optimization. The imported protein structure was determined whether the protein-ligand complex is dimer or multimer and refined the structure to remove redundant binding site. The bond orders were adjusted for untemplated amino acid residues and het group based on the chemical component dictionary (CCD) database. The covalent bond from metal ions and nearby atoms to protein structure changed to zero-order and corrected the formal charges to metal ions and nearby atoms. If the protein structure contains sulfurs close to each other within 3.2 Å, then disulfide bonds were created between two sulfurs. The Prime tool was used to fill missing side chains atoms and loops in protein structure. Finally, in preprocess Epik tool is used to generate the protonation and metal charge states of the het groups at target pH (7.4 ± 2.0) for ligands. Then all water molecules and Het groups from the protein structure were deleted beyond 5.00 Å, and hydrogen atoms were added to the structure. PROPKA tool was used to optimize the H-bond assignment of protein structure at pH 7.0, and the OPLS3e force field was used to constrain energy minimization for energy reduction and protein structure optimization.

Molecular Docking and Receptor grid generation: With receptor grid generation (Maestro v11.8, Schrodinger suite 2018-4), the binding pockets of the protein structure were defined for molecular docking. A literature review, a selection of previously bound protein ligands or sitemap (Maestro v11.8, Schrodinger suite 2018-4) were used to define coordinates (x,y,z) of the cubic grid box. The grid box's length has been increased to 16 Å pixels. The potential of the receptor's nonpolar portions was reduced by a factor of 1.0 Å based on the Van-der Waals radii of non-polar atoms of protein with a partial charge cut-off of 0.25 Å.

The extra precision (XP) Glide (Maestro v11.8, Schrodinger suite 2018-4) was used for induced fit molecular docking of prepared ligands and proteins and utilizing a previously generated receptor grid file. The partial charge was set at a cut-off of 0.15 Å and the scaling factor of 0.80 Å for Vander Waals radii. The ligand sampling was adjusted to flexible docking and included the nitrogen (non-ring) inversions and ring conformations to generate conformers. The bias sampling of the torsions around the bond was also included. The Epik states penalties were added to the docking score.

The XP docking findings were exposed to Prime MM-GBSA (Maestro v11.8, Schrodinger suite 2018-4), which used the VSGB solvation with the force field OPLS3e to determine the binding energies of ligands with protein structures.

Inhibition Constant (Ki): According to the equation below, the inhibition constant was calculated using the binding free energy of the ligand

$$\Delta G = -RT(lnKi) or Ki = e(-\Delta G / RT)$$

Where ΔG is the ligand's binding free energy, R is the gas constant (cal. mol^{-1}. K^{-1}), and T is the ambient temperature (298 Kelvin).

Statistical analysis

The results of the experiments were represented as mean ± standard deviation (S.D.), and sigmoidal dose-response graphs with a nonlinear regression curve fit were used to calculate the median effective concentration (EC_{50}) with a 95% confidence interval (CI). Concentration-response curves were drawn using logarithmic sigmoidal dose-response graphs. For *in vivo* research, one-way ANOVA was used, followed by the Dunnett test and student t-test, with a $p < 0.05$ deemed significant. Graphpad Prism (Version 8.0) and R studio with mainly package "ggplot" was used for all statistical analyses and graph charting

Results

Identification of bioactive compounds by LC-ESI-MS/MS analysis

LC ESI-MS/MS analysis identified 15 bioactive compounds in Cl. EtOH. The major bioactive compounds identified were β-sitosterol, coumarin, gallic acid, catechol, catechin, kaempferol-3-o-glucorhamnoside or kaempferol-7-o-neohesperidoside, vitexin, L-citrulline, protocatechuic acid, ellagic acid, epigallocatechin, vanillin, chlorogenic acid, quercetin, and kaempferol (Fig. 1, Table 1), which may collectively be responsible for this biological activity.

Optimization of HPLC conditions and method validation

The HPLC parameters were optimized with a mobile phase system consisting of solvent A (0.1% TFA in methanol) and solvent B (0.1% TFA in acetonitrile) at a flow rate (0.8 ml/min) was used to achieve the maximum separations and peak visibility of compounds over a 50 ± 5min run time. To enhance the visibility of chromatographic spikes, the retention times of separation peaks were compared to the retention times of external standards under identical chromatographic circumstances at various wavelengths (λ) 250, 280, and 320 nm (Table 2 and Fig. S1). At 280 nm, epigallocatechin and chlorogenic acid peaks were visible; at 320 nm, the peaks of gallic acid, ellagic acid, vanillin, vitexin, and kaempferol were visible, and at 250 nm, the peak of β– sitosterol was visible.

For linearity validation, the calibration curves of dilutions of external standards were employed. The β – sitosterol, epigallocatechin, chlorogenic acid, gallic acid, ellagic acid, vanillin, vitexin, and kaempferol had a linearity range between 1.95 - 500 μg/ml with a significant regression coefficient (r^2) 0.9991-0.9999. LOD and LOQ of the current method were found between 0.25 - 0.81 μg/ml and 0.81 - 2.45 μg/ml, respectively (Table 2). Interday (n = 4) and intraday (n = 12) evaluation of external standards β – sitosterol, epigallocatechin, chlorogenic acid, gallic acid, ellagic acid, vanillin, vitexin, and kaempferol were used to confirm the instrumental precision and repeatability. The precision validation results in Table 2 and Table S1 showed that the interday and intraday %RSDs were 0.83 - 1.41% and 0.64 - 1.75%. To determine the recovery percentage, Cl.EtOH was spiked with various concentrations of external standards (50, 100, and 150 g/ml) in accuracy validation of the instrument. The percentage recovery data (Table 2, Table S2) indicate that the mean value ranges between 98.03 0.88 and 99.42 0.49 with a percent RSD of 0.49 - 1.94%, indicating that this approach is accurate.

Quantification analysis of bioactive compounds by HPLC

Compounds detected by LC ESI-MS/MS were quantified using external standard dilutions and standard calibration curves (Table 2). Kaempferol was present in higher concentration (446.19 μg/g), followed by gallic acid (384.52 μg/g), vitexin (359.88 μg/g), chlorogenic acid (351.2 μg/g), vanillin (335.78 μg/g), and epigallocatechin (314.64 μg/g). Ellagic Acid and β - sitosterol were quantified 289.52 and 251.09 μg/g, respectively.

In vitro experiments

Effects on isolated rat aorta preparation

The Cl.EtOH was applied on intact endothelium aortic preparation to examine the vasorelaxant effect (Fig. S2). The Cl.EtOH exerted the relaxant effect with no constriction in intact endothelium. However, denuded aortic preparations caused the minor constriction at 0.1 to 3 mg/ml, but constrictions relaxed completely at a dose of 5 - 10 mg/ml (Fig. 2A). These constrictions in denuded aortic preparations were blocked with doxazosin (1 μM). Atropine (1 and 3 μM) and L-NAME (1 and 3 μM) were used to blockade the cholinergic and NO induce EDRF based vasorelaxant response on endothelium intact aortic tissue and Cl.

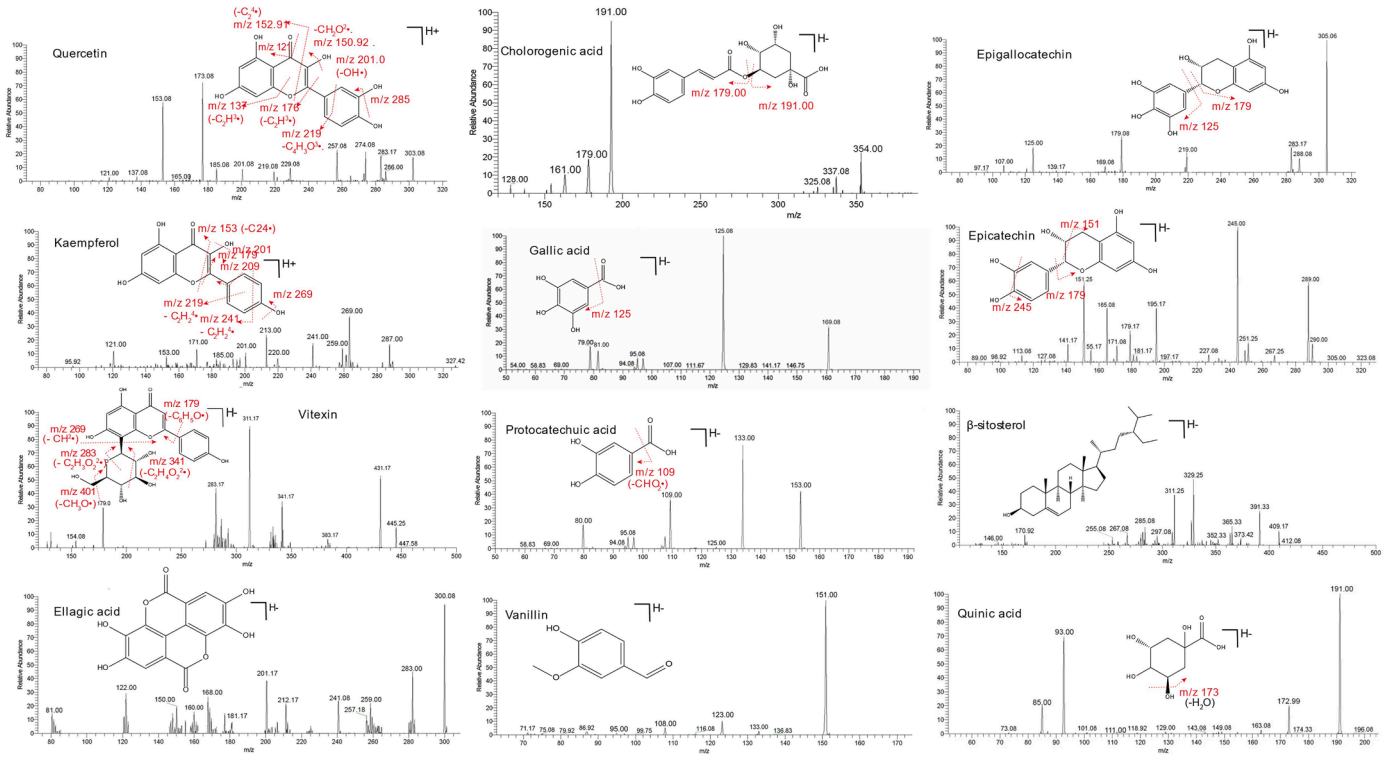

Fig. 1. ESI-MS/MS spectra in negative and positive mode for tentative compounds in Cl.EtOH. The tentative compounds are quercetin, kaempferol, gallic acid, protocatechuic acid, epigallocatechin, and vitexin

EtOH induces constrictions in endothelium intact aortic preparations. The Cl.EtOH induced constrictions in intact endothelium aortic preparations. The Cl.EtOH reverted the phenylephrine (1μM), K^+ (80 mM), and K^+ (25 mM) induced constriction in endothelium and denuded aortic preparations. The EC_{50} for phenylephrine (1 μM), K^+ (80 mM) and K^+ (25 mM) induced constriction on intact endothelium aortic preparations were 0.2429 mg/ml (95% CI: 0.1489 to 0.4071 mg/ml), 6.039 mg/ml (95% CI: 3.161 to 12.97 mg/ml), 0.3295 mg/ml (95% CI: 0.1591 to 0.7633 mg/ml) respectively, whereas EC_{50} for above mentioned contractions on denuded aortic preparations were 1.855 mg/ml (95% CI: 0.6956 to 8.104 mg/ml), 4.030 mg/ml (95% CI: 2.337 to 7.227 mg/ml), 0.1188 mg/ml (95% CI: 0.05380 to 0.2542 mg/ml) respectively (Fig. 2A). In the presence of atropine (1 μM) and L-NAME (1 and 3 μM), Cl.EtOH failed to relax the phenylephrine (1 μM) evoked contractions on intact endothelium aortic tissue. It was observed that atropine (1 μM) completely blocked Cl. EtOH relaxation of the phenylephrine (1 μM) induces contraction on aortic preparations. However, L-NAME (1 μM) failed to block the relaxation but, at 3 μM, the relaxations response of Cl. EtOH was blocked with initial relaxation started at 3 to 10 mg/ml. It indicates the presence of calcium channel antagonistic activity besides the NO-based EDRF mechanism. These results were verified and compared with verapamil, a calcium channel blocker, for possible calcium antagonistic activity of Cl.EtOH. Verapamil relaxed, phenylephrine (1 μM), K^+ (80 mM) and K^+ (25 mM) induced constrictions in intact endothelium aortic preparations with respective EC_{50} of 0.05608 μM (95% Cl: 0.04019 to 0.07924 μM), 0.03896 μM (95% CI: 0.02382 to 0.06550 μM) and 0.01280 μM (95% CI: 0.01072 to 0.01529 μM) respectively (Fig. 2A).

Effect on isolated rat paired atria preparations:

The Cl.EtOH was applied to rat paired atria preparations to explore its possible inotropic and chronotropic effect (Fig. S2). The Cl.EtOH decreased the force of contraction and heart rate in concentration dependent manner at dose 3 - 10 mg/ml with respective EC_{50} of 0.3024 mg/ml (95% CI: 0.1686 to 0.5554 mg/ml) and 0.1213 mg/ml (95% CI: 0.07031 to 0.2067 mg/ml). Atropine (1 μM) attenuated Cl.EtOH negative inotropic and chronotropic effect with respective EC_{50} of 8.794 mg/ml (95% CI: 3.521 to 35.55 mg/ml) and 2.425 mg/ml (95% CI: 1.540 to 3.878 mg/ml) (Fig. 2B). The Cl.EtOH produced the concentration dependent inhibitory response towards force of contraction and heart rate in paired atrium preparation with respective EC_{50} values of 0.02998 μM (95% CI 0.02013 to 0.04510 μM) and 0.3077 μM (95% CI: 0.1969 to 0.4830 μM) (Fig. 2B).

In vivo experiments

Maximum tolerated dose

When Cl.EtOH was studied for a maximum tolerated extract dose in rats. It was found safe with no changes in the body weight, behavioral changes, clinical signs of distress, and mortality of rats were observed during 28 days.

Effect on blood pressure and hemodynamic parameters

The intravenous administration of Cl.EtOH attenuated the dose-dependent systolic blood pressure (SBP), diastolic blood pressure, mean arterial blood pressure (MABP), and pulse pressure with decreased heart beats per min (BPM) in normotensive anesthetized rats (Fig. S3). The hypotensive response of Cl.EtOH was dose-dependent at doses 0.1, 0.3, 0.5, and 1 mg/kg. The Cl.EtOH decreased MABP in range 104, 57, 41, and 55 at respective doses of 0.1, 0.3, 0.5, and 1 mg/kg (Fig. 2C). In the presence of atropine, the hypotensive effect was attenuated, and MABP decreased in the range of 107, 108, 104, 99 at doses 0.1, 0.3, 0.5, and 1 mg/kg, respectively (Fig. 2D). The verapamil decreased MABP in normotensive anesthetized rats in the range of 92, 75, and 53 at respective doses 1, 3, and 10 μg/kg (Fig. 4E).

L-NAME induce acute hypertension

Fig. 4F demonstrated a substantial (p-value < 0.05) rise in MABP (207.808 $\pm$ 5.61 mmHg) in anaesthetized normotensive rats, when treated with L-NAME to induce acute hypertenion. However, treatment

Table 1
Bioactive compounds in Cl.EtOH corresponding to the chromatographic fragments by LC ESI-MS/MS.

Sr. No	Rt (min)	Molecular Weight	Observed MS (m/z)	Calculated MS (m/z)	Error (ppm)	Precursor type	ESI-IT MS/MS (Ions)	Empiricalformula	Proposed compound	Class
1	0.83	414.7	413.3785	413.3781	-0.97	[M-H]-	412.08, 391.33, 365.33, 352.33, 311.25, 297, 285.08, 255.08, 171	$C_{29}H_{50}O$	β-sitosterol	Phytosterols
2	0.97	146.14	147.0441	147.0446	3.40	[M+H]+	147,103, 91, 77	$C_9H_6O_2$	Coumarin	Coumarins
3	2.1	170.12	169.0143	169.0147	2.37	[M-H]-	169, 125, 81, 79	$C_7H_6O_5$	Gallic acid	Hydroxybenzoic acid derivatives
4	2.67	110.11	109.0295	109.0291	-3.67	[M-H]-	109, 108, 81	$C_6H_6O_2$	Catechol	Phenols/ Benzenediols
5	3.12	290.27	291.0863	291.0871	2.75	[M+H]+	291, 165, 139,123	$C_{15}H_{14}O_6$	Catechin	Flavonoid/ Catechins
6	4.3	594.5	593.1512	593.1522	1.69	[M-H]-	593, 327, 285	$C_{27}H_{30}O_{15}$	Kaempferol-3-O-glucorhamnoside / Kaempferol-7-O-neohesperidoside	Flavonoid glycosides
7	5.3	432.4	431.0985	431.0971	-3.25	[M-H]-	431, 341, 311, 283, 117	$C_{21}H_{20}O_{10}$	vitexin	flavone glucoside
8	5.4	175.2	176.1161	176.1163	1.14	[M+H]+	176, 159, 113, 88, 70	$C_6H_{13}N_3O_3$	L- Citrulline	non-essential amino acid
9	5.7	154.12	153.0183	153.0179	-2.61	[M-H]-	153, 109, 91, 80, 65	$C_7H_6O_4$	Protocatechuic acid	Hydroxybenzoic acid derivatives
10	8.8	302.19	300.9993	300.9989	-1.33	[M-H]-	300.08, 283, 257.18,201, 207, 172	$C_{14}H_6O_8$	Ellagic acid	Tannins
11	8.9	306.27	305.0367	305.0377	3.28	[M-H]-	305, 169, 125	$C_{15}H_{14}O_7$	Epigallocatechin	catechin gallates
12	9.5	152.15	151.0411	151.0417	3.97	[M-H]-	151, 136, 123, 108, 95	$C_8H_8O_3$	vanillin	Phenols/ Methoxyphenols
13	11.1	354.31	353.0883	353.0886	0.85	[M-H]-	353, 191, 173	$C_{16}H_{18}O_9$	chlorogenic acid	Alcohols and polyols
14	12.2	302.23	303.0493	303.0483	-3.30	[M-H]+	303, 285, 274, 257, 229, 219, 201, 185, 173, 165, 153, 137	$C_{15}H_{10}O_7$	Quercetin	Flavonoid glycosides
15	16.7	286.23	287.0615	287.0613	-0.70	[M-H]+	287, 269, 263, 259, 241, 213, 201, 185,171, 153, 121	$C_{15}H_{10}O_6$	Kaempferol	Flavanols

Table 2
Quantification and method validation of compounds in Cl.EtOH by HPLC DAD-UV/Vis

Analytes	λ(nm)	Rt (mins)	Linear Regression Data			LOD (μg/ml)	LOQ (μg/ml)	Concentration (μg/g)	Precision (RSD %)		Recovery		Analytes + Extract (μg/g)	
			Range (μg/ml)	Equation	r^2				Inter Day	Intra Day	Mean	RSD %	50 μg	100 μg
β - sitosterol	250	19.5	7.81-500	y = 22.489x + 9.64	0.9999	0.81	2.45	251.09	1.41	0.97	99.42 ± 0.49	0.49	298.14	349.78
Epigallocatechin	280	3.1	7.81-500	y = 259.48x + 14.58	0.9999	0.27	0.81	314.64	0.89	0.64	98.75 ± 1.50	1.52	363.41	412.78
Chlorogenic acid		8.2	7.81-500	y = 239.48x + 12.48	0.9995	0.25	0.75	351.20	0.95	1.75	98.97 ± 1.92	1.94	399.12	450.81
Gallic acid	320	2.4	7.81-500	y = 179.47x + 17.17	0.9998	0.45	1.38	384.52	1.36	0.77	99.23 ± 0.52	0.52	432.92	483.01
Ellagic Acid		7.5	7.81-500	y = 279.53x + 15.56	0.9996	0.26	0.80	289.52	0.83	1.23	98.73 ± 0.88	0.89	337.63	388.15
Vanillin		12.1	7.81-500	y = 202.36x + 14.70	0.9999	0.34	1.04	335.78	1.30	1.06	99.40 ± 0.70	0.71	383.89	433.61
Vitexin		16.2	7.81-500	y = 21.295x + 2.59	0.9993	0.58	1.75	359.88	1.29	1.33	99.35 ± 1.14	1.14	407.76	458.26
Kaempferol		19.4	7.81-500	y = 181.48x + 3.62	0.9999	0.63	1.92	446.19	0.48	1.16	98.57 ± 1.05	1.07	495.77	544.82

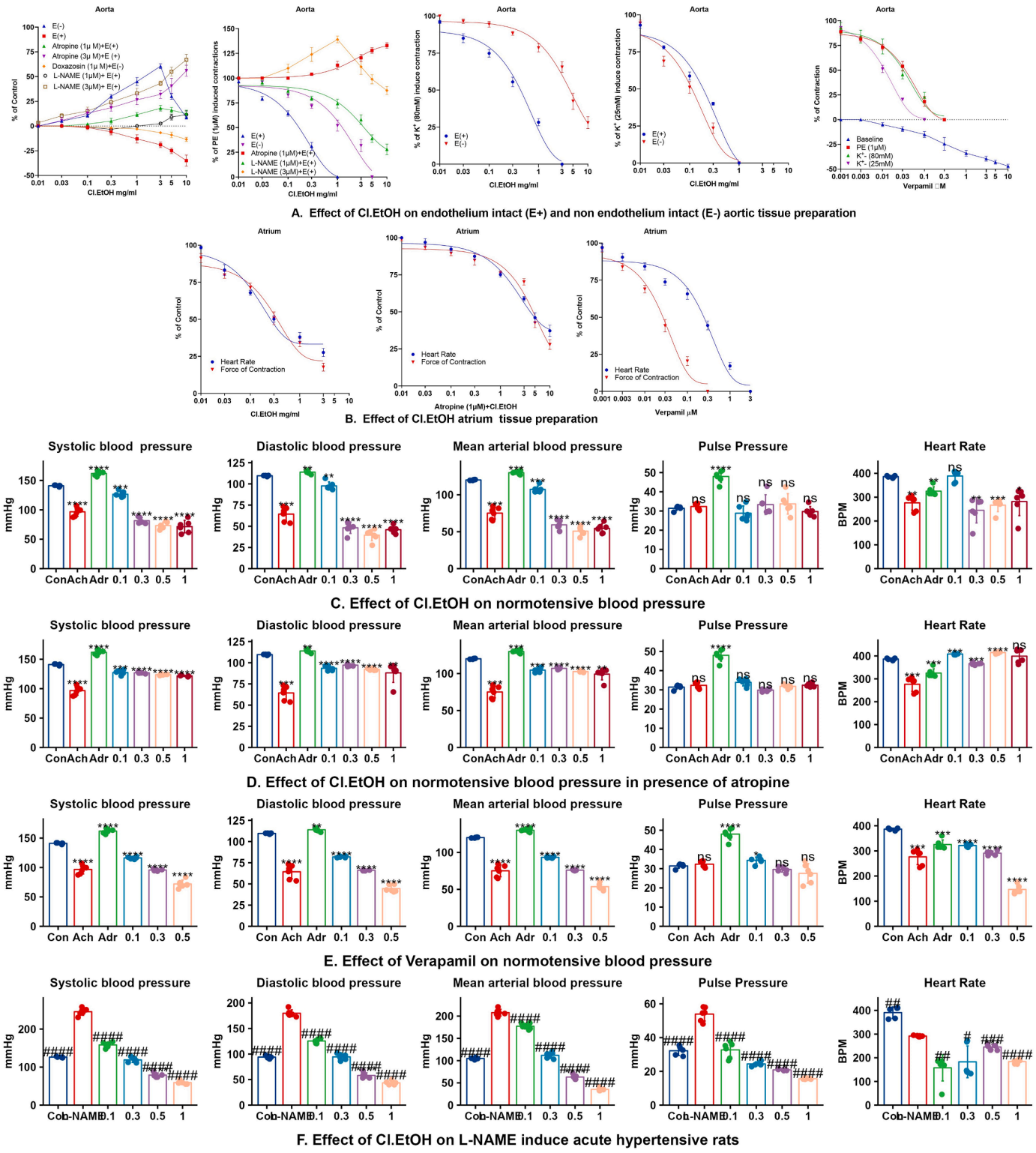

Fig. 2. A. Vasorelaxant effects of Cl.EtOH and verapamil on endothelium intact (E+) and B. denuded endothelium aortic (E-) preparation in phenylephrine (1 μM), K^+ (80 mM), and K+ (25 mM) spastic contractions in the absence and presence of atropine and L-NAME. E. Negative inotropic and positive chronotropic effect of Cl. EtOH on isolated paired atrium preparation in the absence and presence of atropine (1 μM). The hypotensive effect of C. Cl.EtOH (mg/kg) D. in the presence of atropine (1 mg/kg) E. verapamil (μg/kg) in normotensive anesthesia rats and F. on L-NAME induce acute hypertensive rats anesthesia rats with changes in systolic, diastolic, mean atrial blood pressure, pulse pressure (MABP) and heart rate. (Values are expressed as Mean ± S.D., and student t-test was applied and compared to control group and $p < 0.05$ was considered significant). (Values are expressed as Mean ± S.D., and the dose-response curve analyzed data for *in -vitro* experiments (n = 4), *$p < 0.05$, **$p < 0.01$, ***$p < 0.001$, **** $p < 0.0001$ vs control group and #$p < 0.05$, ##$p < 0.01$, ###$p < 0.001$, ####$p < 0.0001$ vs L-NAME group, n = 5). Con: Control, Ach: acetylcholine, Adr: adrenaline

with Cl.EtOH (0.1, 0.3, 0.5, and 1 mg/kg, i.v.) resulted in a signifcant (p-value < 0.05 vs. L-NAME) drop in MABP as 177.37 ± 7.35, 111.8102 ± 3.1, 63.084 ± 2.15 and 36.48 ± 6.165 mmHg at doses 0.1, 0.3, 0.5 and 1 mg/kg.

Effect on ISO induce chronic myocardial injury

The effect of Cl.EtOH on the isoproterenol-induced chronic myocardial injury was studied in different preliminary cardiac hypertrophy indices like biometrical indices, histopathological parameters, and cardiac biochemical markers. It was observed that Cl.EtOH protected the animals from ISO induce chronic myocardial injury.

Physical activity and survival rate

The physical activity and survival rate during the study are major factors indicating myocardial infarction or heart failure. During this study, mortality is expected due to myocardial ischemia. However, no mortality was found in animals treated with Cl.EtOH (75 and 150 mg/kg), verapamil, and carvedilol, but mortality was found in the disease (ISO) group; 3 animals died due to myocardial infarction out of seven animals (Table S3, S4).

In this study, ISO administration decreased the physical activity of rats after the 4^{th} subcutaneous administration of isoproterenol, and it completely diminished after the 10^{th} administration with shortening of breath. At the same time, animals treated with Cl.EtOH (150 mg/kg), verapamil, and carvedilol were active and had neglectable shorting of breath. It was observed that animals in the ISO group lost weight during the study, but increased other parameters like fatigue, shorting of breath, and physical activities were observed. However, weight loss or increase in other parameters was not found in Cl.EtOH (150 mg/kg), verapamil, and carvedilol treatment groups.

Effect on histopathological parameters

The histological changes in myocardial tissue were studied to check necrobiosis with fibroblastic proliferation and inflammatory cells infiltration. Other parameters like the number of cells, diameter, and thickness of both cell and muscle were also studied. The results showed that myocardial tissues of the ISO group had significant damages in muscle fibers (increased fibrosis, inflammatory cells infiltration, local collagen fiber hyperplasia, and interstitial edema of myocardial tissues). Moreover, these tissues had a prominent presence of high neutrophil infiltration, with weak myofibers, pyknosis, karyorrhexis (Fig. 3), and many structurally disordered fibrous tissues. However, Cl.EtOH, verapamil, and carvedilol treatment significantly ($p < 0.05$ vs. ISO group) decreased the inflammatory cells infiltration and fibrosis with less damage in myocardial tissues. The low dose of Cl.EtOH (75 mg/kg) had less significant ($p < 0.05$ vs ISO group) protection. The Cl.EtOH

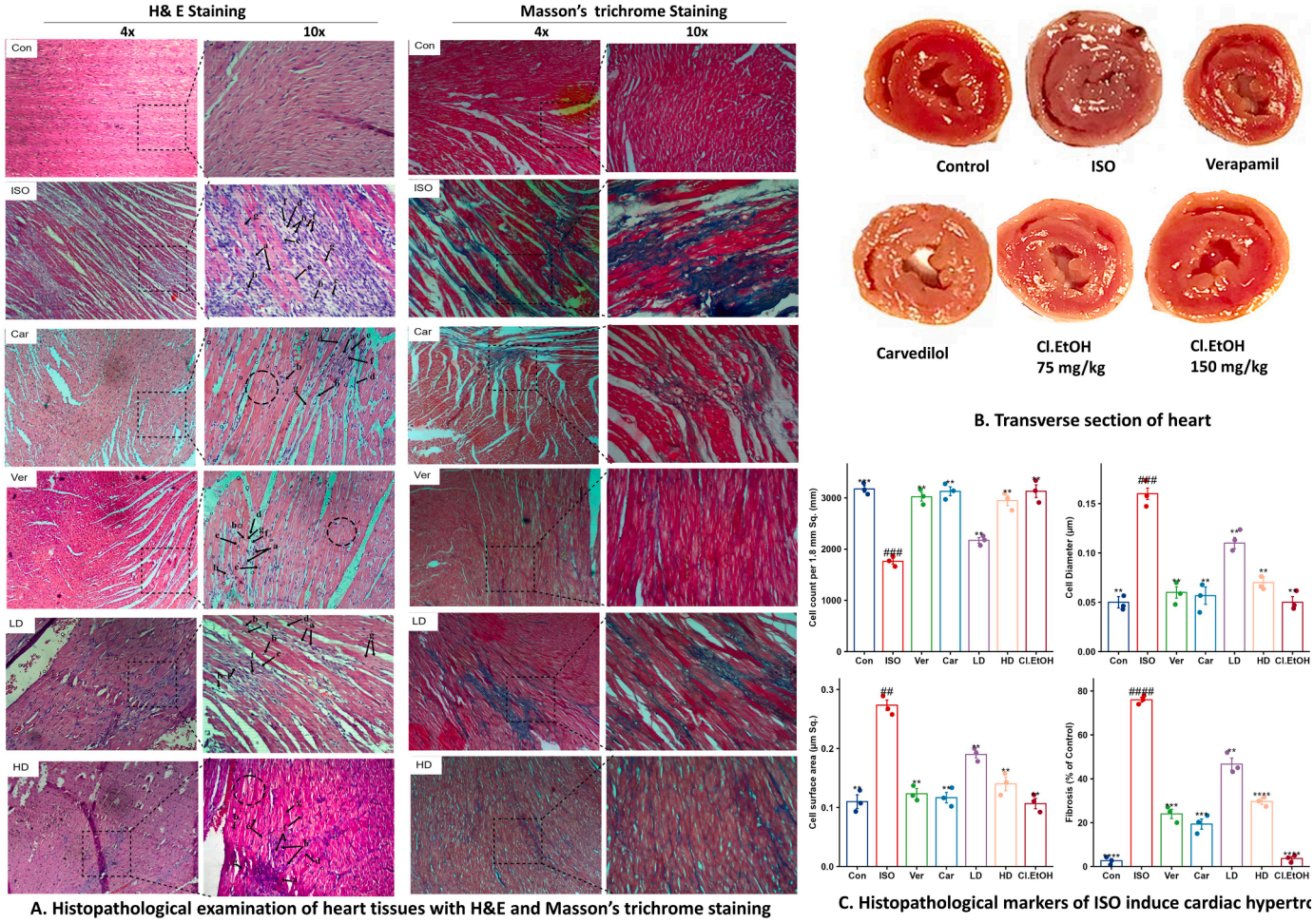

Fig. 3. Effects of Cl.EtOH on gross morphology and histopathological changes in heart tissues. A. Histopathological changes in myocardial tissues of experimental groups after ISO induced MI with hematoxylin-eosin (HE) and Masson's trichrome staining (× 10 magnification); a. Necrotic myocardial fibers; b. Macrophages; c. neutrophil infiltrations; d. Interstitial edema; e. mucoid degeneration; f. fibroblast; g. loss of striations with nuclear changes. B. Gross morphology of heart tissues in transverse section C. The histopathological parameters include cell count, diameter, surface area, and fibrosis. (Values are expressed as Mean ± S.D. (n = 6), *p < 0.05, **p < 0.01, ***p < 0.001, **** p < 0.0001 vs ISO group and #p < 0.05, ##p < 0.01, ###p < 0.001, ####p < 0.0001 vs control group). Con: Control; Ver: verapamil; Car: carvedilol; LD: 75 mg/kg Cl.EtOH; HD: 150 mg/kg Cl.EtOH, Cl.EtOH: 150 mg/kg Cl.EtOH without ISO induced MI,

(150 mg/kg), verapamil, and carvedilol decreased the necrobiosis due to which cell count increased significantly ($p < 0.05$ vs. ISO group).

In contrast, cell diameter and cell surface area were maintained significantly ($p < 0.05$ vs. ISO group), as compared to the ISO group (Fig. 3). These results indicate the Cl.EtOH protects myocardium tissues from ISO-induced infarctions.

Effect on biometrical indices

Fig. 4A depicts the effect of Cl.EtOH on biometrical indices of ISO induced cardiac hypertrophy. It was noticed that ISO administration significantly ($p < 0.05$ vs. control group) increased biometrical indices such as in the disease (ISO) group. All biometrics indices, i.e., heart weight, heart diameter, left heart ventricular (LHV) weight, heart weight index, LHV index, tail length index, and tibia length index, were increased in the ISO group, while Cl.EtOH (150 mg/kg), verapamil, and carvedilol treated groups reduced the biometrical indices. These treated groups had significance ($p < 0.05$ vs. ISO group) protection from cardiac hypertrophy as compared to the ISO group, while no significant ($p < 0.05$ vs. control group) difference was observed between control and these treated groups. The low dose (75 mg/kg) of Cl.EtOH was found with low significance ($p < 0.05$ vs. ISO group) protection in animals.

The gross investigation of LHV thickness showed the significant ($p < 0.05$ vs. control group) presence of hypertrophy in the ISO group (Fig. 3C, 4A) as compared to the control group, however, Cl.EtOH (150 mg/kg), verapamil, and carvedilol treated groups had no remarkable thickness.

Effect on serum cardiac biochemical markers

The serum biochemical markers, especially CK, CK-MB, cTnT, cTnI, LDH, ANP, and lipid profile, have clinical significance in myocardial

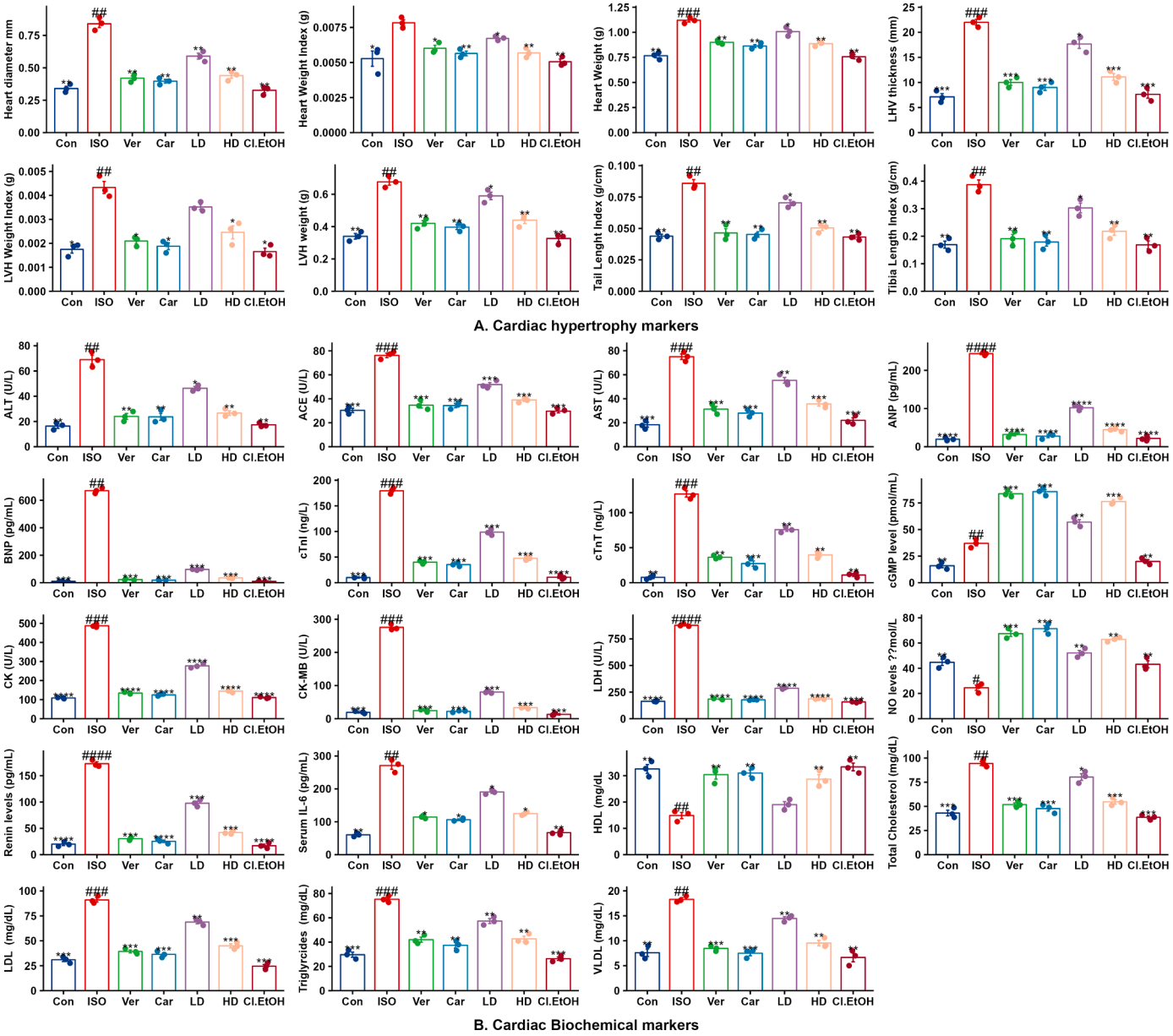

Fig. 4. Effects of Cl.EtOH on hypertrophic and myocardial infarction biochemical markers. A. The biometric cardiac hypertrophy markers B. The changes in serum biochemical cardiac makers after ISO induced MI. (Values are expressed as Mean ± S.D (n = 6), data were analyzed by student t-test, compared to ISO group, whereas ISO group compared with control and $p < 0.05$ was considered significant. *$p < 0.05$, **$p < 0.01$, ***$p < 0.001$, **** $p < 0.0001$ vs ISO group and #$p < 0.05$, ##$p < 0.01$, ###$p < 0.001$, ####$p < 0.0001$ vs control group). Con: Control; ISO: isoprenaline; Ver: verapamil; Car: carvedilol; LD: 75 mg/kg Cl.EtOH; HD: 150 mg/kg Cl.EtOH, Cl.EtOH: 150 mg/kg Cl.EtOH without ISO induce MI,

infarction diagnosis. Besides, other serum biomarkers help study cardiac injuries such as ACE, NO concentrations, renin concentrations, ALT, AST, serum IL-6, BNP, and cGMP concentrations. Fig. 4B showed that there was a significant ($p < 0.05$ vs. control group) difference between ISO and control biomarkers. The rise of these serum biomarkers in the ISO administrated group indicates chronic myocardial infarction, although Cl.EtOH (150 mg/kg), verapamil, and carvedilol treated groups, had serum biomarkers within the limit range except low dose (75 mg/kg) of Cl.EtOH. These treated groups had significance ($p < 0.05$ vs. ISO group) protection from myocardial infarction as compared to the ISO group and no significant ($p < 0.05$ vs. control group) difference between control and these treated groups. The results showed that Cl. EtOH protects the animals from ISO-induced cardiotoxicity.

Gene expression analysis

Fig. 5 presented the mRNA expression of inflammatory and cardiac genes such as NOS3, ANP, IL-6, cTnT, and MMP-9 were studied. mRNA expression of ANP, IL-6, MMP-9, and cTnT was significantly down-regulated in Cl ($p < 0.05$ vs. ISO group).EtOH (150 mg/kg), verapamil, and carvedilol treated myocardium, but the expression of these genes significantly ($p < 0.05$ vs. control group) increased in the ISO group. The low dose (75 mg/kg) of Cl.EtOH was found with low significance ($p < 0.05$ vs. ISO group). However, mRNA expression of NOS3 was significantly ($p < 0.05$ vs. ISO group) up-regulated in Cl.EtOH (150 mg/kg), verapamil, and carvedilol treated cardiac tissues, whereas its expression was significantly ($p < 0.05$ vs. control group) reduced in hypertrophied hearts of the ISO group.

The hierarchical clustering heatmap analysis was used to determine the normalized intensities of gene expression in ISO, control, Cl.EtOH (75 and 150 mg/kg), verapamil, and carvedilol (Fig. 5B). The results indicate that the tendency of expression in treatment groups was far from the expression of the ISO group but near the control group. Furthermore, these results demonstrated that Cl.EtOH successfully reversed and changed gene expression trends similar to verapamil and carvedilol.

With western blot analysis, we found that IL-6 and MMP-9 expression were decreased in Cl.EtOH (150 mg/kg), carvedilol, and verapamil compared to the ISO group, where they were increased. When IL-6 and MMP-9 expression were increased, it indicated inflammation in cardiomyocytes. However, NOS3 expression was increased in Cl.EtOH (150 mg/kg), carvedilol, and verapamil compared to the ISO group where NOS3 was decreased. When NOS3 expression increased, it indicated the relaxation in cardiomyocytes (Fig. 5C, Fig. S4). The hierarchical clustering heatmap analysis indicate that Cl.EtOH successfully reversed the tendency of protein expression in treatment groups and clustered the ISO group far away from treated groups (Fig. 5D).

Metabolomics profiling analysis

Multivariate data analysis

The principal component 1 and 2 were utilized to score the PCA plot.

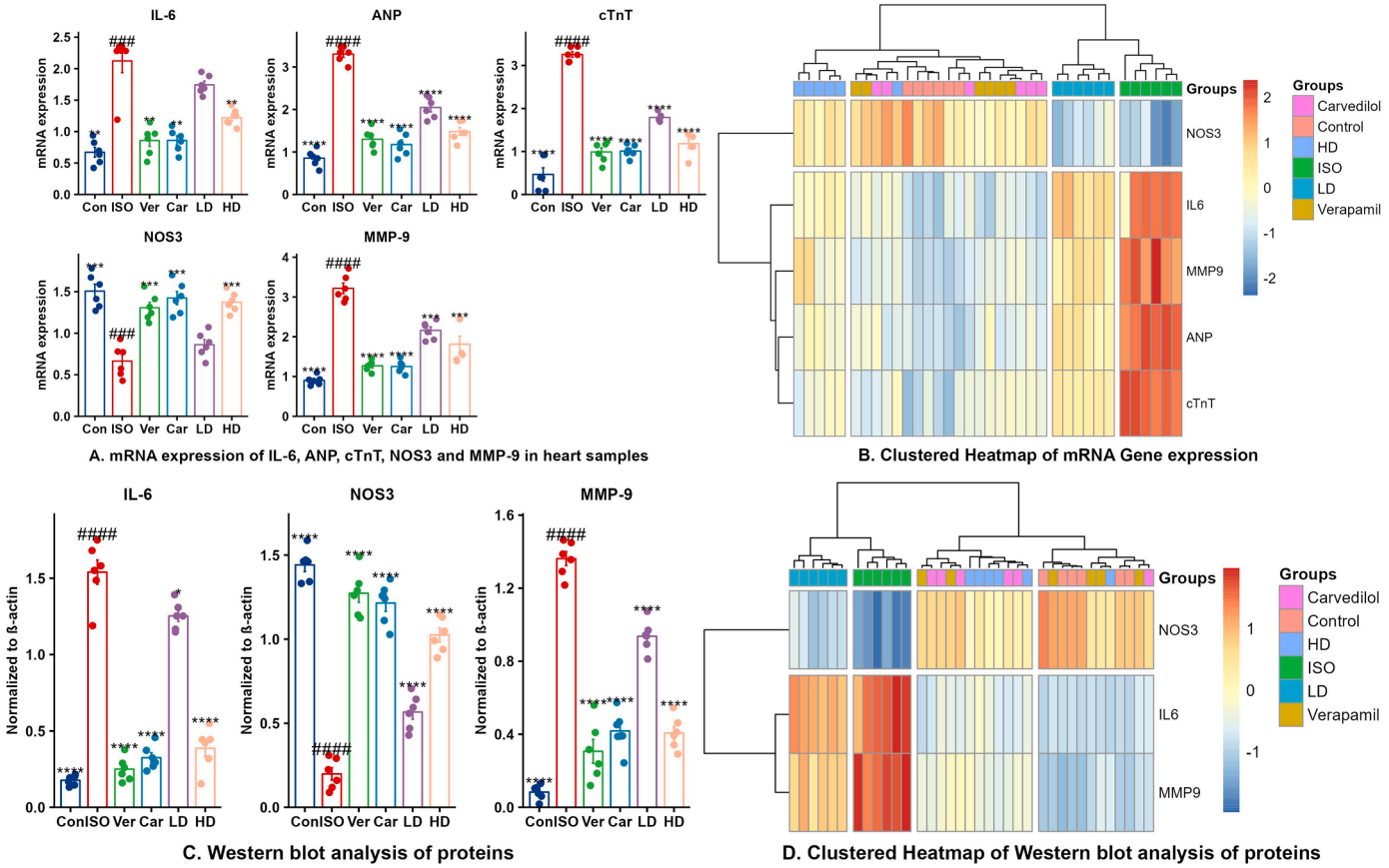

Fig. 5. Effects of Cl.EtOH on mRNA gene expressions of IL-6, ANP, cTnT, NOS3, and MMP-9 in myocardial tissues after ISO induced MI. A. The trend of gene expression in hypertrophy myocardial tissues B. The hierarchical clustering heatmap analysis of gene expression in myocardial tissues; red represented the increase in gene expression while blue represented the decrease. C. Western Blot analysis of NOS3, MMP9 and IL-6. β-actin used as housekeeping genes. D. The hierarchical clustering heatmap analysis of protein expression in myocardial tissues; red represented the increase in gene expression while blue represented the decrease. (Values are expressed as Mean ± S.D (n = 6), data were analyzed by student t-test, compared to ISO group, whereas ISO group compared with control and $p < 0.05$ was considered significant. *$p < 0.05$, **$p < 0.01$, ***$p < 0.001$, ****$p < 0.0001$ vs ISO group and #$p < 0.05$, ##$p < 0.01$, ###$p < 0.001$, ####$p < 0.0001$ vs control group). Con: Control; ISO: isoprenaline; Ver: verapamil; Car: carvedilol; LD: 75 mg/kg Cl.EtOH; HD: 150 mg/kg Cl.EtOH.

The unsupervised PCA score plots of metabolome data of serum (R^2X = 0.976, Q^2= 0.963) and heart (R^2X = 0.997, Q^2= 0.992) showed a satisfactory classification of experimental groups with an explicit separation between ISO group and others groups, i.e., Cl.EtOH (150 mg/kg), verapamil, and carvedilol (Fig. S5). If R^2X and Q^2 are more significant than 0.5, the model is considered good stability and prediction. These results indicate a successful modeling process with severe metabolic alteration in the ISO group.

The supervised OPLS-DA plot was used to discriminate the serum and heart metabolites between control, ISO, Cl.EtOH (150 mg/kg), verapamil, and carvedilol groups. In the OPLS-DA plot, there was explicit serum and heart metabolites discrimination between the ISO group and others groups, i.e., Cl.EtOH (150 mg/kg), verapamil and carvedilol. The ISO group was far away from the Cl.EtOH (150 mg/kg), verapamil, and carvedilol treated groups whereas Cl.EtOH (150 mg/kg), verapamil, and carvedilol treated groups intersect each other (Fig. 8). The higher R^2X, Q^2, and CV-ANOVA parameters of the model indicated the excellent fitness and predictability of OPLS-DA patterns without overfitting. The OPLS-DA models of serum ($R^2X = 0.967$, $Q^2 = 0.695$) and myocardium tissues ($R^2X = 0.997$, $Q^2 = 0.627$) had good stability and predication. So, OPLS-DA analysis results indicate a significant difference ($p < 0.05$) between metabolites of ISO and treated groups. Furthermore, OPLS-DA models between control and ISO (serum: $R^2X = 0.989$, $Q^2 = 0.999$; heart: $R^2X = 0.977$, Q^2= 0.912), verapamil (serum: $R^2X = 0.853$, $Q^2 = 0.743$; heart: $R^2X = 0.994$, $Q^2 = 0.776$), and EtOH extract (150 mg/kg) (serum: $R^2X = 0.976$, $Q^2 = 0.997$; heart: $R^2X = 0.969$, $Q^2 = 0.738$) were established for both serum and heart metabolites and also OPLS-DA model was established for verapamil and Cl.EtOH (150 mg/kg) (serum: $R^2X = 0.957$, $Q^2 = 0.992$; heart: $R^2X = 0.980$, $Q^2 = 0.334$).

For statistically validity and significance of serum and cardiac tissue metabolites of control, Cl.EtOH (150 mg/kg), verapamil, carvedilol and ISO group were further evaluated by permutation tests with cross

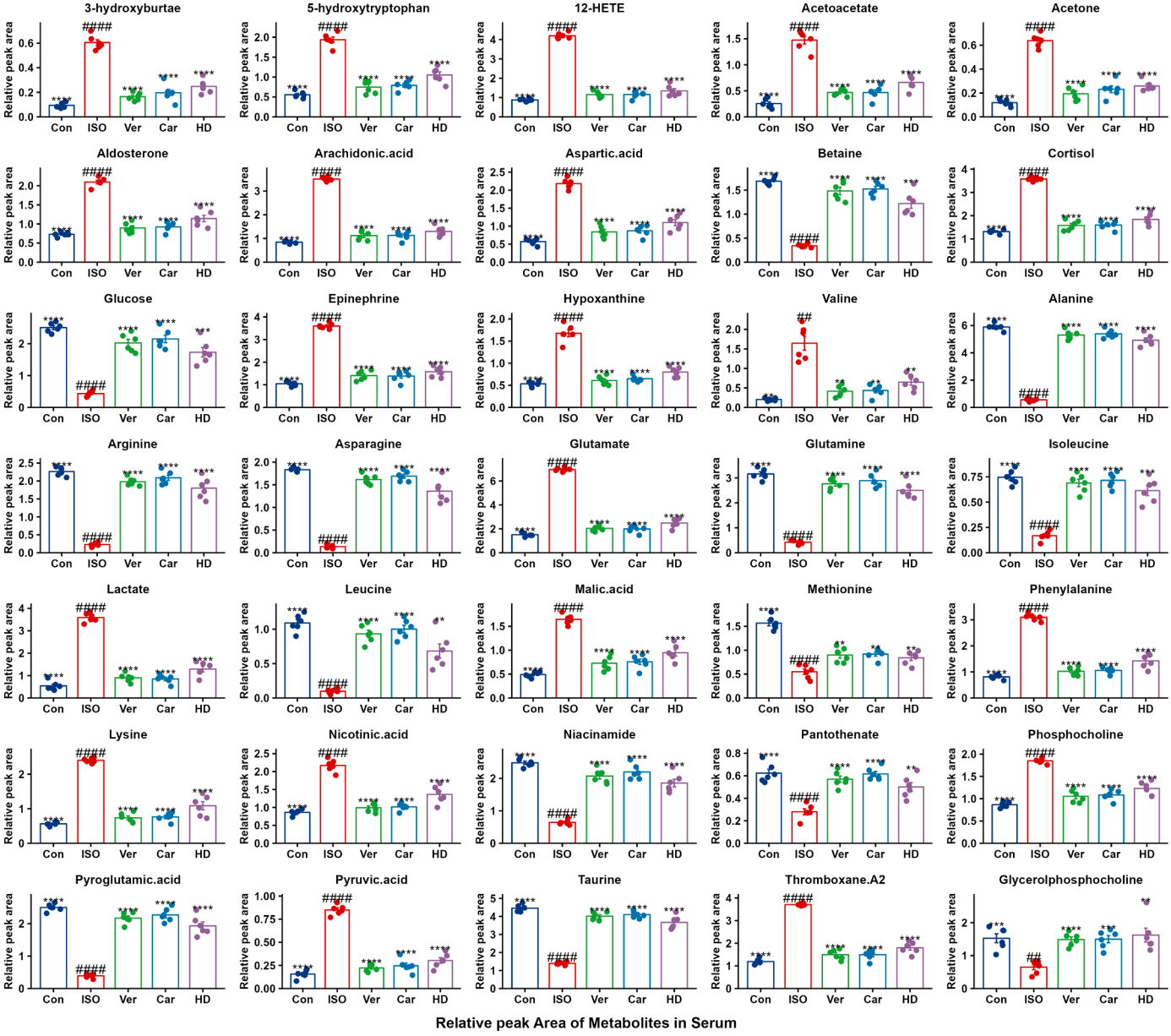

Fig. 6. Effects of Cl.EtOH on metabolic profiles of serum samples after ISO induced MI. A. The trend metabolic profiles of serum samples. (Values are expressed as Mean ± S.D (n = 6)), data were analyzed by student t-test, compared to ISO group, whereas ISO group compared with control and $p < 0.05$ was considered significant. *$p < 0.05$, **$p < 0.01$, ***$p < 0.001$, ****$p < 0.0001$ vs ISO group and #$p < 0.05$, ##$p < 0.01$, ###$p < 0.001$, ####$p < 0.0001$ vs control group). Con: Control; ISO: isoprenaline; Ver: verapamil; Car: carvedilol; HD: 150 mg/kg Cl.EtOH

validation (Fig. S5). The parameter R^2 used for variance and Q^2 explains the predictability of model, degree of overlapping and correlation between permutated and original data. The negative Q^2 intercept suggested the good predictability and correlation of model. The permutation test results for serum ($R^2 = 0.251$, $Q^2 = -0.50$ and cardiac tissues ($R^2 = 0.075$, $Q^2 = -0.524$) indicate that models are stable and predicated the variation. Furthermore, validation models between control and ISO (serum: $r^2x = 0.409$, $q^2 = -0.918$; heart: $r^2x = 0.947$, $q^2 = -0.913$), verapamil (serum: $r^2x = 0.328$, $q^2 = -1.31$; heart: $r^2x = 0.437$, $q^2 = -0.908$), and Cl.EtOH (150 mg/kg) (serum: $r^2x = 0.584$, $q^2 = -2.25$; heart: $r^2x = 0.214$ $q^2 = -0.629$) were established for both serum and heart metabolites and also validation model was established for verapamil and Cl.EtOH (150 mg/kg) (serum: $r^2x = 0.482$, $q^2 = -2.37$; heart: $R^2X = 0.209$, $Q^2 = -0.512$).

Analysis of the biomarkers in different samples

Serum metabolites: The metabolome data analysis was used to identify the metabolites and explore the metabolic pathways related to myocardial infarction. In serum, 75 metabolites as potential biomarkers were filtered and identified, including ketone bodies, mineralocorticoid, eicosanoids, organic acids, amino acids, glycoproteins, choline, glycerol, glucose, and betaine. Fig. 6 depicts the alternation of 35 metabolites in serum. The levels of 3-hydroxybutyrate, 5-hydroxytryptophan, 9-HETE, acetoacetate, acetone, aldosterone, arachidonic acid, aspartic acid, betaine, cortisol, glucose, epinephrine, hypoxanthine, valine, lactate, malic acid, phenylalanine, lysine nicotinic acid, phosphocholine, pyruvic acid, and thromboxane A2 were significantly ($p < 0.05$, vs. control group) elevated in ISO group as compared to control. However, Cl.EtOH (150 mg/kg), verapamil, and carvedilol significantly ($p < 0.05$, vs. ISO group) reversed and inhibited alternation of these metabolites

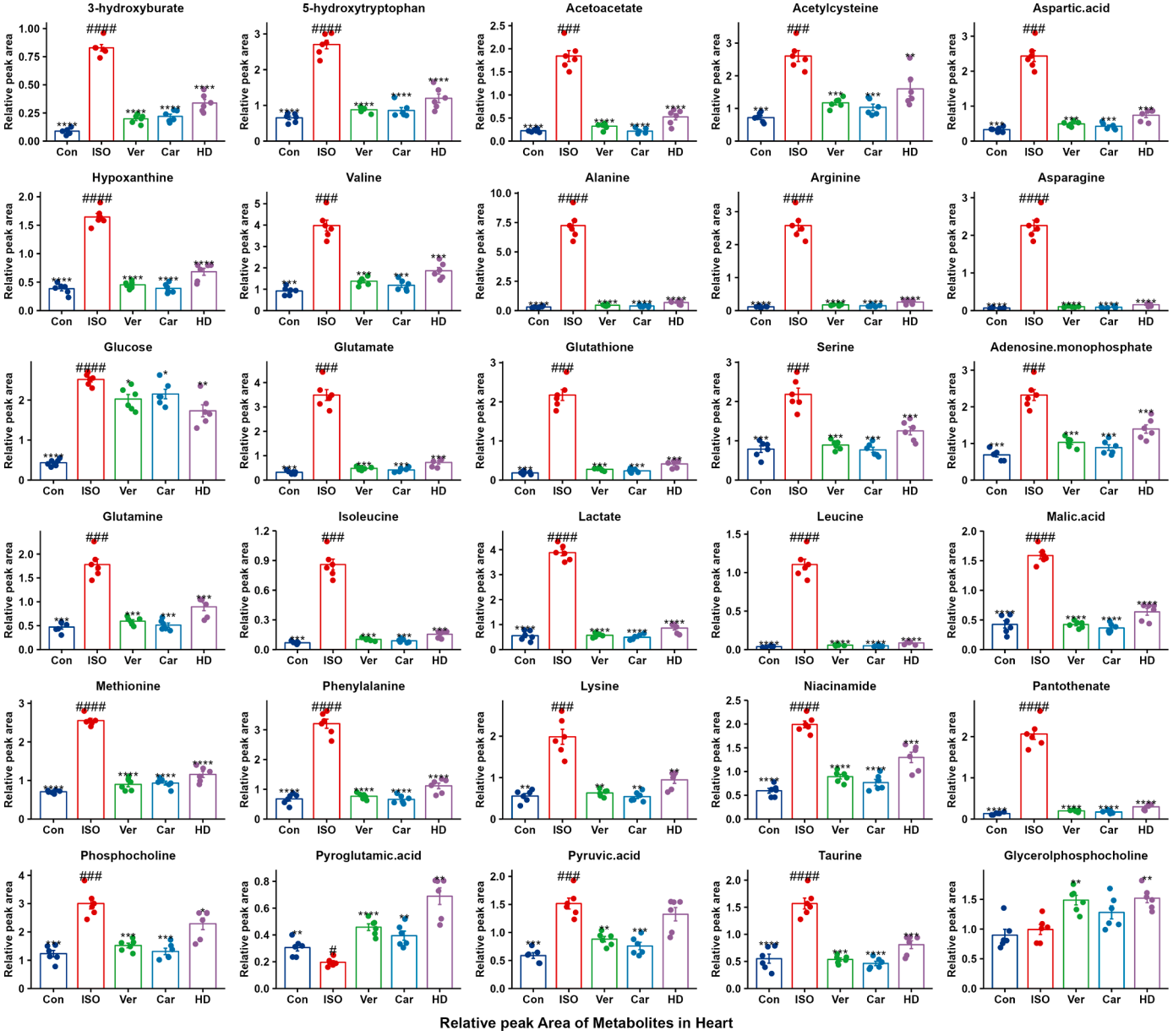

Fig. 7. Effects of Cl.EtOH on metabolic profiles of heart samples after ISO induced MI. A. The trend metabolic profiles of heart tissue sample. (Values are expressed as Mean ± S.D (n = 6)), data were analyzed by student t-test, compared to ISO group, whereas ISO group compared with control and $p < 0.05$ was considered significant. *$p < 0.05$, **$p < 0.01$, ***$p < 0.001$, ****$p < 0.0001$ vs ISO group and #$p < 0.05$, ##$p < 0.01$, ###$p < 0.001$, ####$p < 0.0001$ vs control group). Con: Control; ISO: isoprenaline, Ver: verapamil; Car: carvedilol; HD: 150 mg/kg Cl.EtOH

expressions in rats. However, it was observed that amino acids, i.e., alanine, arginine, asparagine, glutamate, glutamine, isoleucine, leucine, methionine, niacinamide, pantothenate, pyroglutamic acid, taurine, and glycerol phosphocholine significantly ($p < 0.05$ vs. control) reduced as compared to control in ISO group, whereas Cl.EtOH (150 mg/kg), verapamil, and carvedilol significantly ($p < 0.05$ vs. ISO group) improved amino acids expressions. These results showed that Cl.EtOH (150 mg/kg) ameliorated alternation of isoproterenol-induced myocardial infarction in rats similar to verapamil and carvedilol.

Heart tissue metabolites: In cardiac tissue, 60 potential metabolites biomarkers were filtered and identified. Fig. 7 portrayed the alternation of 30 metabolites in the heart. The results indicated that levels of 3-hydroxybutyrate, 5-hydroxytryptophan, acetoacetate, acetylcysteine, aspartic acid, hypoxanthine, valine, alanine, arginine, asparagine, glucose, glutamate, glutathione, serine, adenosine monophosphate, glutamine, isoleucine, lactate, leucine, malic acid, methionine, phenylalanine, lysine, niacinamide, pantothenate, phosphocholine, pyroglutamic acid, pyruvic acid, taurine, glycerol phosphocholine were significantly ($p < 0.05$, vs. control group) elevated in ISO group as compared to control, but Cl.EtOH (150 mg/kg), verapamil and carvedilol significantly ($p < 0.05$, vs. ISO group) reversed and inhibited alternation of these metabolites expressions in rats.

Metabolic pathway analysis

The serum metabolites were subjected to MetaboAnalyst to identify the pathway enrichment and metabolic pathways relevant to myocardial infarction. Total 46 metabolic pathways were identified in serum and 38 in heart tissues. Fig. 8 illustrated that the ISO group had highly altered metabolic pathways with higher concentrations of metabolites than control, but verapamil and Cl.EtOH (150 mg/kg) regulated the concentration of the metabolite and had a minor alteration in metabolic pathways to treat myocardial injury. The above-mentioned metabolic pathways mainly involve energy, amino acid, and oxidative metabolism stress. Notably, amino acid and energy metabolism pathways were significantly enriched in the ISO group and then reversed with Cl.EtOH (150 mg/kg) and verapamil treatment, especially BCAAs, glutamine, and glutamate metabolisms ketone bodies, and amino acid degradation.

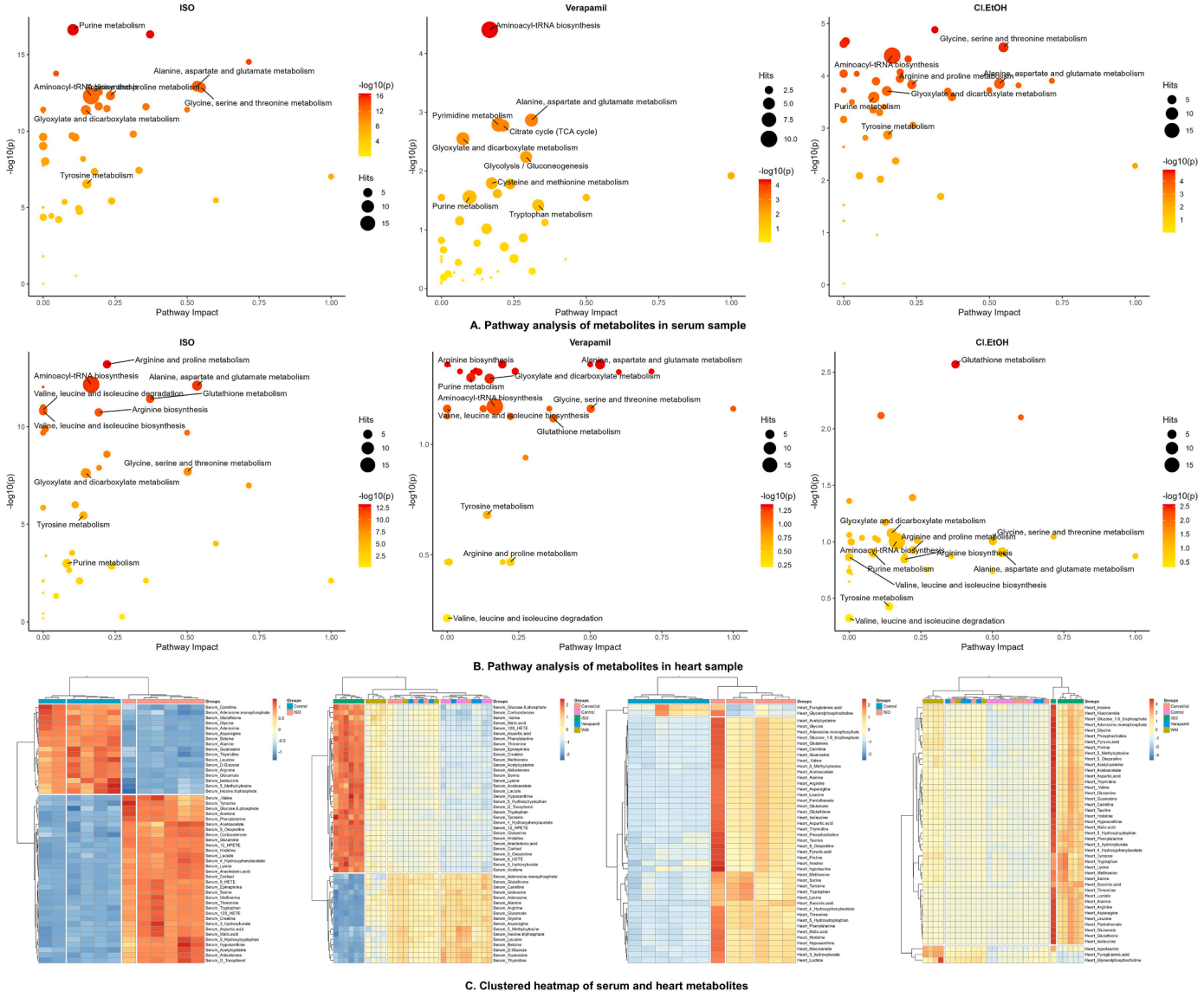

Fig. 8. Summary of metabolic pathways analysis. Metabolic Pathway analysis of ISO, verapamil, and Cl.EtOH in A. serum and B. heart. The data were normalized with the control group. The size and color of each circle represented the significance (p-value) of metabolic pathway and pathway impact, respectively. The red indicated the higher p-value, and the yellow represented the lower p values. C. The hierarchical clustering heatmap analysis for the alterations of metabolites in serum and heart samples after ISO induces MI between control, ISO, verapamil, carvedilol, and Cl.EtOH (150 mg/kg).

Thus, metabolic pathway analysis illustrated the cardioprotective mechanism of Cl.EtOH (150 mg/kg).

Correlation and Heatmap analysis of metabolites

The heatmap analysis and correlation approaches were used to narrow the significance and accurate predictability of Cl.EtOH effectiveness between ISO and treated groups. First, heatmap correlation analysis based on the Pearson correlation coefficient was used to recognize the relationship among the altered metabolites (Fig. 9).

The hierarchical clustering heatmap analysis was employed to determine the normalized intensities of endogenous metabolites in ISO, control, Cl.EtOH (150 mg/kg), verapamil, and carvedilol (Fig. 8). The results indicate that the tendency of metabolites in treatment groups was far away from the metabolites of the ISO group but near the control group. Furthermore, these results demonstrated that Cl.EtOH successfully reversed and changed the trends of metabolites similar to verapamil and carvedilol.

Molecular docking

Docking calculations are advantageous for predicting the position of a ligand inside a target protein's binding site. The use of physical energy factors (i.e., solvation energy) in conjunction with an appropriate force field improves th e accuracy of docking calculations for compounds (Kuhn and Kollman, 2000; Sirous et al., 2019). The beneficial effects of bioactive compounds from Cl.EtOH, epigallocatechin, vitexin, gallic acid, vanillin, and chlorogenic acid were docked with target proteins with voltage-gated calcium channel β2a (VGCC, PDB:1T0J), Muscarinic receptor 3 (PDB ID: 5ZHP), and nitric oxide synthase 3 (NOS3, PDB: 1M9R) to validate the activities as represented in Table 3 and Fig. 10. These proteins are members of EDRF, and calcium mediate signaling pathways (Eschenhagen, 2018).

Voltage-gated calcium channel β2a: Vitexin had dominant binding energies for voltage-gated calcium channels ($\Delta G_{Binding}$: -48.43 kcal/mol). It formed conventional hydrogen bond interaction with amino acids residues Arg65 (2.17 Å), Arg227 (3.01 Å), Lys90 (1.96 Å), Asp384 (2.01 Å), Gln380 (1.85 Å), Phe383 (2.98 Å), and Val109 (1.69 Å), carbon hydrogen bond interaction with residues Arg65 (2.38 Å), Asp384 (2.70 Å), Gln380 (2.96 Å), Glu381 (2.46 Å), and Asp384 (2.64 Å), π-π T-shaped interaction with residue Phe92 (5.15 Å), and π-alkyl interaction with residues Lys90 (4.63 Å). Chlorogenic acid scored the second rank for VGCC with binding affinity -28.41 kcal/mol. It had hydrogen bond interaction with amino acid residues Asp319 (1.88 Å), Asp319 (2.17 Å), and Ile261 (3.06 Å), π-donor hydrogen bond interaction with residue Ile263 (3.31 Å), and salt bridge / electrostatic attractive charge interaction with residue Lys254 (2.25 Å), electrostatic attractive charge interaction with residue Lys247 (4.27 Å), and π-alkyl interaction with residue Ile263 (4.45 Å). The rank of ligands with VGCC based on docking score are given below: vitexin, chlorogenic acid, epigallocatechin, gallic acid, and vanillin.

Muscarinic receptor 3: Chlorogenic acid scored lowest binding affinity for Muscarinic receptor 3 (-46.39kcal/mol). It formed hydrogen bond interaction with amino acids residues Ile222 (1.94 Å), Tyr506 (2.34 Å), Lys522 (2.33 Å), Cys220 (2.55 Å), Cys220 (2.02 Å), Leu225 (1.68 Å), and Asn513 (1.63 Å), carbon hydrogen bond interaction with residues Phe221 (2.96 Å), Pro228 (2.66 Å), Pro228 (2.57 Å), Thr231 (2.86 Å), and Cys220 (2.98 Å), electrostatic attractive charge interaction with residue Lys522 (4.91 Å), electrostatic π-anion interaction with residue Trp525 (4.75 Å), π-σ interaction with residue Thr231 (2.65 Å), and π-alkyl interaction with residue Tyr529 (4.52 Å). Vitexin scored the second rank for M_3 receptor with binding affinity -41.07 kcal/mol. It had hydrogen bond interaction with amino acid Tyr148 (1.88 Å), Lys522

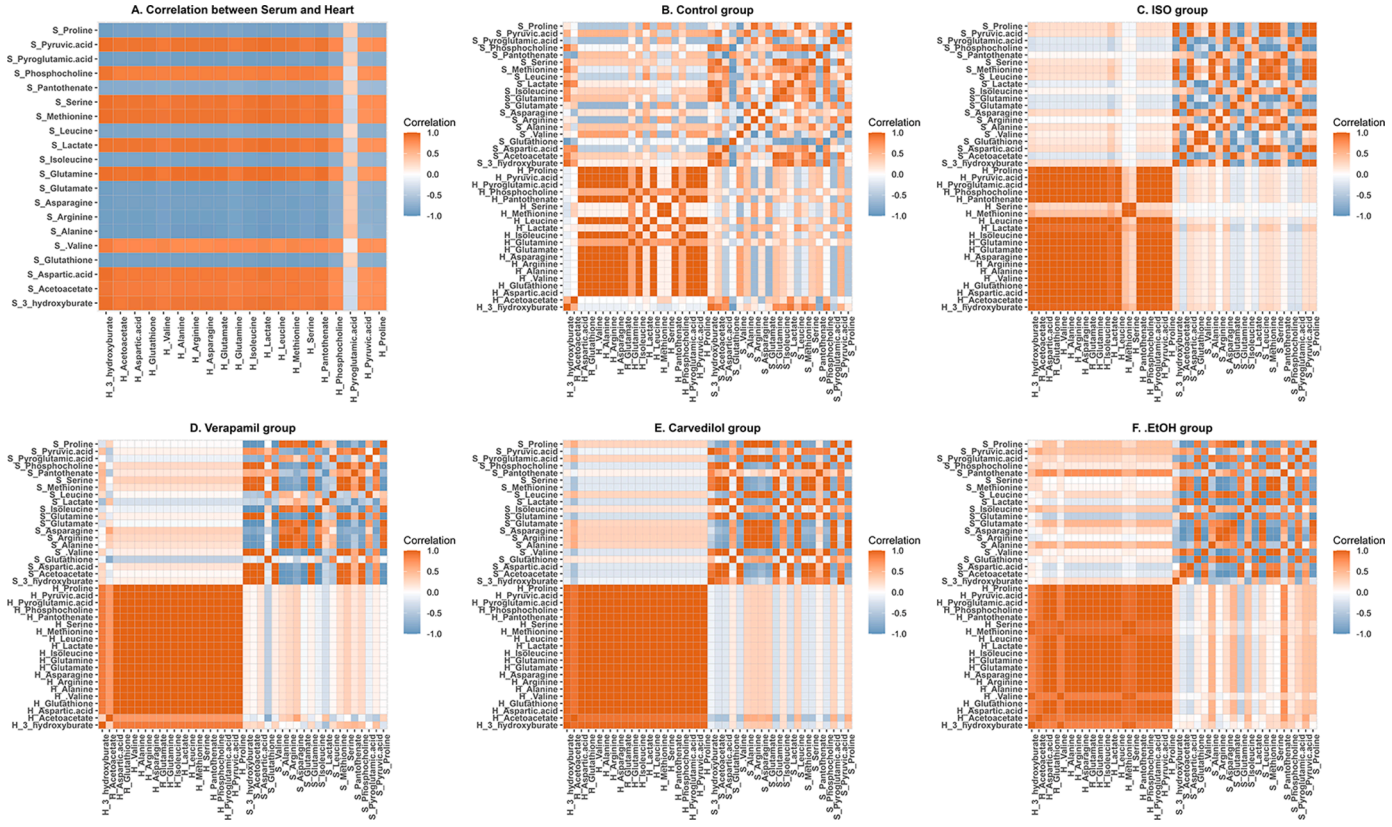

Fig. 9. Correlation Heatmap analysis of serum and heart metabolites varied significantly after ISO induced MI. A. Correlation between serum and heart metabolites. Correlation Heatmap analysis of serum and heart metabolites in B. Control group, C. ISO group, D. Verapamil group, E. Carvedilol group F. Cl.EtOH (150 mg/kg) group. S: Metabolites identified in the serum; H: Metabolites identified in the heart.

Table 3
Binding energies (kcal/mol) of compounds with voltage-gated calcium channel beta2a, muscarinic receptor 3, and nitric oxide synthase 3 calculated by Prime MMGBSA

Name	Docking score	$\Delta G_{Binding}$	Log (pK_i) (μM)	$\Delta G_{Coulomb}$	$\Delta G_{Covalent}$	ΔG_{Hbond}	$\Delta G_{Lipophilic}$	$\Delta G_{Solv\ GB}$	ΔG_{vdW}	Residue-Ligand Interactions with Distance (Å) **Hydrogen Bonds**	**Electrostatic / Hydrophobic Bonds**
Voltage-gated calcium channel beta2a (PDB:1T0J)											
Vitexin	-6.61 ± 0.14	-48.59 ± 1.00	-17.80	-40.91	5.46	-3.29	-9.9	40.04	-39.06	**Conventional Hydrogen Bond:** Arg65 (2.17), Arg227 (3.01), Lys90 (1.96), Asp384 (2.01), Gln380 (1.85), Phe383 (2.98), Val109 (1.69), **Carbon Hydrogen** Bond: Arg65 (2.38), Asp384 (2.70), Gln380 (2.96), Glu381 (2.46), Asp384 (2.64),	**π- π T-Shaped:** Phe92 (5.15), **Pi-Alkyl:** Lys90 (4.63)
Chlorogenic acid	-5.86 ± 0.13	-28.50 ± 0.58	-9.11	-0.33	0.96	-3.46	-9.88	15.54	-30.34	**Conventional Hydrogen Bond:** Asp319 (1.88), Asp319 (2.17), Ile261 (3.06), **π -Donor Hydrogen Bond:** Ile263 (3.31),	**Salt Bridge; Electrostatic Attractive Charge:** Lys254 (2.25), **Electrostatic Attractive Charge:** Lys247 (4.27), Pi-Alkyl: Ile263 (4.45)
Epigallocatechin	-5.82 ± 0.12	-37.51 ± 0.77	-13.01	-40.45	3.27	-4.2	-7.07	40.4	-28.07	**Conventional Hydrogen Bond:** Arg227 (2.34), Gln380 (1.87), Pro336 (2.04), Glu381 (2.24), Pro336 (2.18**), Carbon Hydrogen Bond:** Ser330 (2.66),	**Electrostatic π -Cation:** Arg65 (4.30), Arg227 (4.66), **Electrostatic π -Anion:** Asp384 (3.79), Asp384 (4.70)
Gallic acid	-3.29 ± 0.07	-9.41 ± 0.19	-0.84	1.03	-0.09	-2.42	-2.95	8.02	-12.95	**Conventional Hydrogen Bond:** Asp251	
Vanillin	-2.86 ± 0.06	-25.28 ± 0.52	-7.72	-16.48	1.13	-1.83	-8.14	15.07	-13.44	**Conventional Hydrogen** Bond: Phe92 (1.87),Arg227 (2.36),	**π- π T-Shaped:** Phe92 (5.18)
Verapamil	-2.54 ± 0.05	-44.60 ± 0.91	-16.08	-19.55	3.75	-1.21	-14.26	29.51	-41.79	**Conventional Hydrogen Bond:** Arg227 (2.65) **Carbon Hydrogen Bond:** Tyr402 (2.72), Asp384 (2.54), Tyr402 (2.69), Glu111 (2.61), Ser330 (2.75), Pro336 (2.49), Glu381 (2.67), Ser382 (2.43)	**Electrostatic Attractive Charge:** Asp384 (4.51) **π -Cation:** Arg227 (4.00) **π-Anion:** Asp384 (3.66) **Alkyl:** Ala335 (4.32), Ala405 (3.99), Lys110 (4.24), Pro326 (5.46), Ile338 (4.46) **π-Alkyl:** Phe92 (5.37), Lys110 (5.11), Ala409 (4.44))
Muscarinic receptor 3 (PDB ID: 5ZHP)											
Chlorogenic acid	-11.25 ± 0.24	-46.85 ± 1.00	-16.92	-59.66	9.72	-3.75	-18.41	66.62	-39.63	**Conventional Hydrogen Bond**: Ile222 (1.94), Tyr506 (2.34), Lys522 (2.33), Cys220 (2.55), Cys220 (2.02), Leu225 (1.68), Asn513 (1.63), **Carbon Hydrogen Bond:** Phe221 (2.96), Pro228 (2.66), Pro228	**Electrostatic Attractive Charge: Lys522** (4.91), **π -Anion**: Trp525 (4.75), **π -σ**: Thr231 (2.65), **π -Alkyl:** Tyr529 (4.52),

(*continued on next page*)

Table 3 (*continued*)

Name	Docking score	$\Delta G_{Binding}$	Log (pK_i) (μM)	$\Delta G_{Coulomb}$	$\Delta G_{Covalent}$	ΔG_{Hbond}	$\Delta G_{Lipophilic}$	$\Delta G_{Solv\ GB}$	ΔG_{vdW}	Residue-Ligand Interactions with Distance (Å) **Hydrogen Bonds**	**Electrostatic / Hydrophobic Bonds**
										(2.57), Thr231 (2.86), Cys220 (2.98),	
Vitexin	-8.28 ± 0.18	-41.48 ± 0.89	-14.61	-29.92	7.72	-2.3	-10.32	28.87	-32.99	**Conventional Hydrogen** Bond: Tyr148 (1.88), Lys522 (2.06), Cys220 (2.32), Asn513 (1.71), **π -Donor Hydrogen Bond:**Phe221 (2.73), Trp525 (2.52),	**π - π T-Shaped:** Trp525 (4.90),
Epigallocatechin	-7.85 ± 0.17	-38.76 ± 0.83	-13.44	-21.83	2.9	-3.19	-13.59	26.97	-29.12	**Conventional Hydrogen Bond:** Ile222 (2.68), Tyr506 (2.41), Lys522 (2.40), Ile222 (2.19), Cys220 (1.74), Cys220 (2.12), **Carbon Hydrogen Bond:** Ser226 (2.47), Lys522 (2.53), Tyr148 (2.91),	
Gallic acid	-6.66 ± 0.14	-19.83 ± 0.42	-5.30	-39.36	1.65	-2.69	-10.44	49.65	-16.14	**Conventional Hydrogen** Bond: Tyr148 (1.87), Ile222 (2.66), Cys220 (1.67), Asn526 (2.31) **Carbon Hydrogen Bond**: Phe221 (2.59)	
Vanillin	-4.75 ± 0.10	-32.33 ± 0.69	-10.67	-9.48	4.62	-1.31	-11.28	7.24	-19.84	**Conventional Hydrogen Bond:** Tyr506 (1.83), Cys220 (1.97),	**Alkyl:** Leu144 (4.69), **π -Alkyl:** Trp143 (4.66),
Verapamil	-2.29 ± 0.05	-62.00 ± 1.33	-23.43	2.45	4.92	-1.22	-27.11	2.8	-41.13	**Conventional Hydrogen Bond:** Ile222 (2.45), Lys522 (2.03), **Carbon Hydrogen Bond:** Phe221 (2.73), Lys522 (2.42), Asn513 (3.04), Glu219 (2.69), Glu219 (2.63), Cys220 (3.03), Cys220 (2.66), Ile222 (2.53)	**Electrostatic π -Cation:** Trp525 (4.66), Trp525 (4.11), **π -Donor Hydrogen Bond:** Tyr506 (2.95), **π- π Stacked**: Phe221 (4.95), Tyr529 (5.24), **Alkyl:** Ile222 (4.67), Leu225 (4.88), Leu144 (4.82), **π -Alkyl:** Tyr127 (4.92), Trp143 (4.55), Phe221 (4.41), Tyr529 (5.05)
Nitric oxide synthase 3 (NOS3, PDB: 1M9R)											
Epigallocatechin	-9.75 ± 0.20	-25.85 ± 0.55	-7.88	-35.34	7	-4.15	-22.25	53.78	-18.81	**Conventional Hydrogen Bond:** Arg365 (2.70), Ala446 (1.67), Ser102 (1.80), His461 (2.13), Trp447 (2.88), Val449 (2.27), Glu361 (1.87), Glu361 (1.76), **Carbon Hydrogen Bond:** Pro451 (2.41), Ala446 (2.30)	**Electrostatic π -Cation:** Arg365 (3.31), Pi-Pi Stacked: Trp447 (5.93), Trp447 (4.46), Trp447 (5.15), **Alkyl:** Ala446 (5.17), **π -Alkyl:** Trp445 (5.28), Phe460 (4.72), Trp447 (4.28), Trp447 (3.93), Val104 (5.06), Pro451 (5.41)
Vitexin	-8.04 ± 0.16	-45.07 ± 0.96	-16.15	-28.62	5.78	-4.33	-11.28	51.64	-47.15	**Conventional Hydrogen Bond:** Arg365 (2.12), Arg365 (1.99), Arg365 (2.60),	**Electrostatic Pi-Cation:** Arg365 (3.78), Arg365 (4.67), Arg365 (4.30), **Pi-Pi**

(*continued on next page*)

Table 3 (*continued*)

Name	Docking score	$\Delta G_{Binding}$	Log (pK_i) (μM)	$\Delta G_{Coulomb}$	$\Delta G_{Covalent}$	ΔG_{Hbond}	$\Delta G_{Lipophilic}$	$\Delta G_{Solv\ GB}$	ΔG_{vdW}	Residue-Ligand Interactions with Distance (Å) **Hydrogen Bonds**	**Electrostatic / Hydrophobic Bonds**
										Arg372 (2.67), Glu361 (2.02), Glu361 (2.01), Phe460 (2.51), Glu361 (2.77), **Carbon Hydrogen Bond:** Glu361 (2.77), **π -Donor Hydrogen Bond:** Trp74 (3.22),	**Stacked:** Phe460 (4.70), Trp447 (4.13), Trp447 (5.52), Trp447 (4.84), Trp447 (4.45), Trp447 (5.44), **π- π T-Shaped:** Trp74 (5.47), Pi-Alkyl: Val104 (4.58),
Gallic acid	-7.81 ± 0.16	-1.82 ± 0.04	2.45	-35.42	2.04	-3.62	-13.41	78.48	-25.1	**Conventional Hydrogen Bond:** Arg365 (1.95), Arg365 (2.17), Ser102 (1.76), Ala446 (2.41), Ser102 (2.24),	**Electrostatic Attractive Charge:** Arg365 (3.35), **π - π Stacked:** Trp447 (5.26), Trp447 (4.43), **Pi-Alkyl:** Val104 (5.13),
Vanillin	-6.41 ± 0.13	-26.04 ± 0.56	-7.97	-10.21	1.28	-1.24	-15.66	30.3	-26.5	**Conventional Hydrogen Bond:** Arg365 (2.05), Ser102 (1.77), **Carbon Hydrogen Bond:** Ala446 (2.44),	**π- π Stacked:** Trp445 (5.34), Trp445 (5.50), Trp447 (5.83), Trp447 (4.88), **π - π T-Shaped:** Phe460 (5.46), **π -Alkyl:** Phe460 (4.84), Trp447 (3.40), Trp447 (3.67), Val104 (5.07),
Chlorogenic acid	-2.93 ± 0.06	-42.91 ± 0.92	-15.22	-53.59	6.98	-4.77	-22.33	72.94	-39.25	**Conventional Hydrogen Bond:** Arg365 (1.99), Arg365 (2.54), His371 (2.83), Trp447 (2.35), Glu361 (1.78), Glu361 (1.94),	**Electrostatic Attractive Charge:** Arg183 (4.59), **π- π Stacked:** Trp447 (4.81), **π- Alkyl:** Pro451 (4.91),
Verapamil	-1.41 ± 0.03	-57.41 ± 1.23	-21.46	34.01	2.66	-0.88	-32.07	0.19	-55.17	**Carbon Hydrogen Bond:** Trp447 (2.39), Trp447 (2.58), Trp447 (2.58), Val449 (2.69), Glu361 (2.86), Glu361 (2.67), Ser102 (3.00), Phe460 (2.70),	**Electrostatic Attractive Charge**: Glu361 (4.20), **Electrostatic π-Cation:** Arg365 (4.74), **Electrostatic π-Anion:** Glu361 (3.52), **π-π Stacked:** Phe460 (4.90), Trp447 (4.04), Trp447 (4.33), **Alkyl:** Val104 (5.02), **π-Alkyl:** Trp74 (4.73), Trp445 (4.32), Trp445 (4.37), Trp447 (5.22), Trp447 (4.02)

Values are expressed as Means ± S.D, n = 3, **$\Delta G_{Binding}$:** Binding free energy, **Log (pKi):** Logarithmic of predicated Inhibition Constant (pK_i), **$\Delta G_{Coulomb}$:** Coulomb binding energy, **$\Delta G_{Covalent}$:** Covalent binding energy **ΔG_{Hbond}:** Hydrogen bonding energy, **$\Delta G_{Lipophilic}$:** Lipophillic binding energy, **$\Delta G_{Solv\ GB}$:** Generalized born electrostatic solvation energy **ΔG_{vdW}:** Van der Waals forces energy. These all energy contribute to Binding free energy (**$\Delta G_{Binding}$**)

(2.06 Å), Cys220 (2.32 Å), and Asn513 (1.71 Å), π-donor hydrogen bond interaction with residues Phe221 (2.73 Å), and Trp525 (2.52 Å), and π-π T-shaped interaction with residue Trp525 (4.90 Å). The rank of ligands with a muscarinic receptor based on docking score is given below: chlorogenic acid, vitexin, epigallocatechin, gallic acid, and vanillin.

Nitric oxide synthase 3: Vitexin hit the lowest binding energy for (ΔGBinding: -44.62 kcal/mol) for NOS3 but scored the second position on the docking score (-8.012 kcal/mol). It formed hydrogen bond interaction with amino acid residues Arg365 (2.12 Å), Arg365 (1.99 Å), Arg365 (2.60 Å), Arg372 (2.67 Å), Glu361 (2.02 Å), Glu361 (2.01 Å), Phe460 (2.51 Å), and Glu361 (2.77 Å), carbon hydrogen bond interaction with residue Glu361 (2.77 Å), π-donor hydrogen bond interaction with residue Trp74 (3.22 Å), electrostatic π-cation interaction with residues Arg365 (3.78 Å), Arg365 (4.67 Å), and Arg365 (4.30 Å), π-π stacked interaction with residue Phe460 (4.70 Å), Trp447 (4.13 Å), Trp447 (5.52 Å), Trp447 (4.84 Å), Trp447 (4.45 Å), and Trp447 (5.44 Å), π-π T-Shaped interaction with residue Trp74 (5.47 Å), and π-alkyl interaction with residue Val104 (4.58 Å). Epigallocatechin first in docking score (-9.72 kcal/mol) with binding affinity -25.59 kcal/mol. It formed hydrogen bond interaction with amino acid residues Arg365 (2.70 Å), Ala446 (1.67 Å), Ser102 (1.80 Å), His461 (2.13 Å), Trp447 (2.88 Å), Val449 (2.27 Å), Glu361 (1.87 Å), and Glu361 (1.76 Å), carbon hydrogen bond interaction with residues Pro451 (2.41 Å), and Ala446 (2.30 Å), electrostatic π-cation interaction with residue Arg365 (3.31 Å),

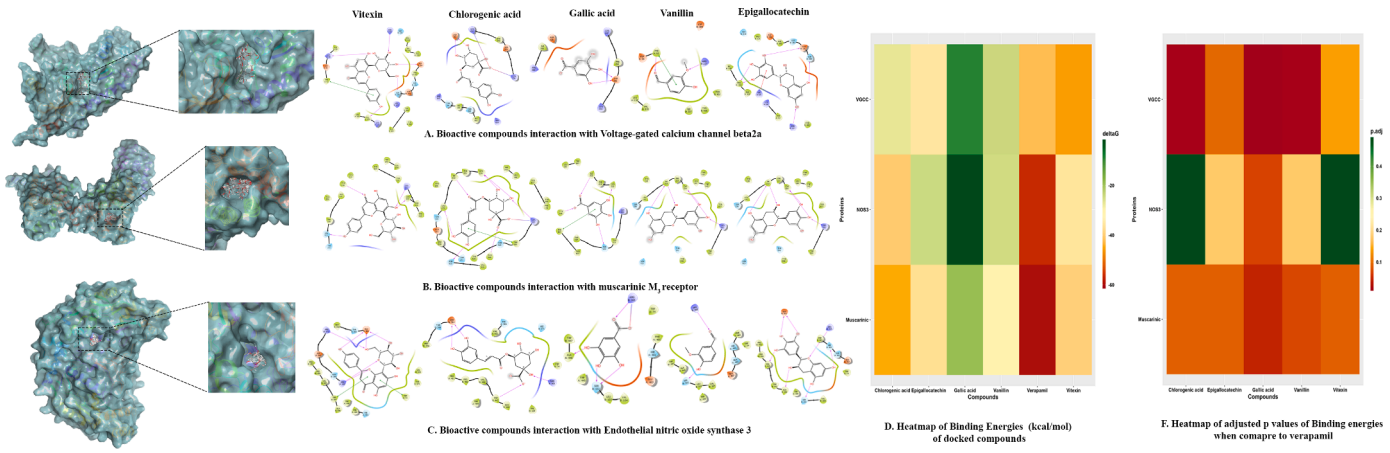

Fig. 10. Depicted the 2D protein-ligand interaction between bioactive compounds (vitexin, chlorogenic acid, epigallocatechin, gallic acid, and vanillin) and proteins; A. voltage-gated calcium channel β2a (VGCC, PDB:1T0J), B. muscarinic receptor 3 (PDB ID: 5ZHP), C. nitric oxide synthase 3 (NOS3, PDB: 1M9R). D. Heatmap of binding energies (kcal/mol), of bioactive compounds (rutin, quercetin, scopoletin, and kaempferol) and proteins. E. Heatmap of p-adjusted values of binding energies when compared to verapamil. ($p < 0.05$ vs verapamil).

π-π stacked interaction with residue Trp447 (5.93 Å), Trp447 (4.46 Å), and Trp447 (5.15 Å), alkyl interaction with residue Ala446 (5.17 Å), and π-alkyl interaction with residues Trp445 (5.28 Å), Phe460 (4.72 Å), Trp447 (4.28 Å), Trp447 (3.93 Å), Val104 (5.06 Å), and Pro451 (5.41 Å).

Chlorogenic acid was second to vitexin found with binding affinity -42.49 kcal/mol but had the last position in docking score. It formed hydrogen bond interaction with amino acid residues Arg365 (1.99 Å), Arg365 (2.54 Å), His371 (2.83 Å), Trp447 (2.35 Å), Glu361 (1.78 Å), and Glu361 (1.94 Å), electrostatic attractive charge interaction with residue Arg183 (4.59 Å), π-π stacked interaction with residue Trp447 (4.81 Å), and π-alkyl interaction with residue Pro451 (4.91 Å). The rank of ligands with NOS3 based on docking score is given below epigallocatechin, vitexin, gallic acid, vanillin, and chlorogenic acid.

Discussion

The seeds and fruit of *Citrullus lanatus* (Thunb.) Matsum. & Nakai. have been regarded as traditional healers and used to treat various diseases. *C. lanatus* seeds have been used for centuries to bolster and enhance health, as an energy booster, and treat cardiovascular disorders. Still, its therapeutic actions for CVDs remain unknown. However, more research is necessary to fully comprehend the impact of *C. lanatus* seeds on vasorelaxation and myocardial violations. (Rajasree et al., 2016; Siddiqui et al., 2018). As a result, this work used an integrated method of metabolomics profiling to investigate putative pathways of *C. lanatus* in isoproterenol (ISO)-induced myocardial infarction (MI). Isoproterenol causes long-lasting cardiac hypertrophy by causing cardiomyocyte compensatory loss, which may progress to heart failure. The LC-ESI MS/MS screening of Cl.EtOH revealed that major bioactive compounds are β-sitosterol, coumarin, gallic acid, catechol, catechin, vitexin, L- citrulline, protocatechuic acid, ellagic acid, epigallocatechin, vanillin, chlorogenic acid, quercetin, kaempferol. The rutin, kaempferol, and quercetin exert antispasmodic activity (Gilani et al., 2008).

Vasorelaxant response through the blockade of VGCC: The Cl.EtOH was tested for possible vasorelaxant activity on intact endothelium and denuded rat aortic preparations. On both preparations, the Cl.EtOH had a vasorelaxant effect. Like verapamil, Cl.EtOH displayed a relaxant response to PE (1 μM), and K^+ (80 mM) produced contractions. PE activates 1-adrenergic receptors, prompting phosphatidylinositol to be converted to inositol-1,4,5-triphosphate, which raises intracellular calcium via triggering voltage-dependent calcium channels. The sympathetic nervous system regulates the vascular smooth muscle tone (Sharkey and MacNaughton, 2018). Adrenoceptors promote stimulatory actions in vascular smooth muscle by raising cytosolic calcium levels, either by the inflow of calcium from extracellular fluid or release from cytosolic reserves, to elicit depolarization of vascular preparations resting action potentials. The Cl.EtOH in our study suppressed K^+ (80 mM) and K^+ (25 mM) spastic contractions at 5 mg/ml and 1 mg/ml, respectively, whether it intervenes by calcium channel blockade or potassium channel opening. K^+ (80mM) triggered depolarization with the inflow of calcium current into the cell, increasing cytosolic calcium ions, and this intense depolarized membrane action may have resulted in a long-lasting persistent contractile response in aortic preparations. (Saqib and Janbaz, 2016). The smooth muscle will relax after repolarization has occurred by blocking the influx of calcium current, Cl.EtOH relaxed the K^+ (80 mM) induced contraction and blocked the evoked depolarization and repolarized membrane potential. The following events were expected to be inhibited (Sharkey and MacNaughton, 2018). The following series of events were expected to be inhibited: 1) decreased in cytosolic calcium ions concentration, 2) the insufficient cytosolic calcium ions to interact with the regulating protein phosphokinase C, the calcium-calmodulin complex could not form., 3); myosin light chain kinase (MLCK) activation and MLCs phosphorylation did not occur and 4) The interaction of actin and phosphorylated MLCs did not occur; As a result, the tissue contractile response was not attained (Saqib and Janbaz, 2016; Wahid et al., 2021).

Consequently, Cl.EtOH and verapamil completely blocked K^+ (80 mM) and K^+ (25 mM) induced contractions (Mehmood et al., 2014). The relaxation of PE (1 μM) and K^+ (80 mM) generated contractions reflects a blockage of intracellular calcium influx through calcium channels. Calcium channel blockers (CCB) are essential medications to treat angina and hypertension (Saqib and Janbaz, 2016). Literature data describes epicatechin, apigenin, quercetin, rutin and caffeic acid having antispasmodic activity (Lanuzza et al., 2017). It was previously reported that the antispasmodic activity of epicatechin (Ghayur et al., 2007), naringenin, kaempferol, quercetin, and rutin (Ajay et al., 2003; Fusi et al., 2003; Gilani et al., 2006) on isolated aorta preparation.

Vasorelaxant response through the regulation of NO: As mentioned above, Cl.EtOH also relaxed PE-induced spastic contraction on both endothelium (intact and denuded) aortic preparations. However, in the presence of atropine and L-NAME, it failed to relax the PE-induced spastic contractions on endothelium intact aortic portion. Hence, nitric oxide (NO), an endothelium-derived vasodilator, may be released consequence of muscarinic receptors activation located in vascular endothelium. NO activates guanylyl cyclase and produces cGMP from cGTP. Subsequently, intracellular concentrations of cGMP increase, triggering the cGMP-dependent protein kinase, which intervenes with

inositol 1,4,5-triphosphate receptor-associated cGMP kinase substrate and MLC phosphatase, leads decrease intracellular calcium concentration and decrease the availability of MLC for actin and MLC cross-bridge for vasoconstriction (Fig. 11).

The development of oxidative stress-related hypertension is linked to decreased NO bioavailability. Oxidative stress is a pro-hypertensive factor that worsens endothelial dysfunction and increases vasoconstriction, all of which lead to increased systemic vascular resistance and elevated blood pressure (Touyz et al., 2018). Nitric oxide synthase catalyzes the production of endogenous nitric oxide (NO) from the amino acid L-arginine (NOS). NO reduces adrenergic neurotransmission and lowers NADPH oxidase-driven superoxide anion (O2•), in addition to working directly on vascular smooth muscle cells to produce relaxation. Endothelial dysfunction in the presence of L-NAME may be caused through the oxidation of NO by O2• to the potent oxidant peroxynitrite (ONOO) (Kukongviriyapan et al., 2015). Endothelial NOS (eNOS) uncoupling is caused by ONOO molecules, leading to the generation of O2• instead of NO. ONOO also inhibits eNOS activation by inhibiting eNOS phosphorylation by protein kinase B (Akt) (Aekthammarat et al., 2019). We discovered that in the presence of L-NAME, endothelium-dependent vasorelaxation of Cl.EtOH in the aortic preparation was attenuated, indicating endothelial dysfunction. Cl.EtOH treatment, interestingly, reduced endothelial dysfunction while also lowering oxidative stress, probably due to its antioxidant action.

Negative inotropic and chronotropic effect: When Cl.EtOH studied rat paired atrium, it exhibited the negative inotropic and chronotropic effect, the diminished force of contraction, and partial decrease in heart rate. The heart muscle contraction is introduced by the electrical excitation of cardiac myocytes (excitation-contraction coupling, ECC). The plausible explanation of observed findings is that Cl.EtOH may be exhibited through cholinergic activity or blockade of adrenoceptors and L-type calcium ion channels (Eschenhagen, 2018). In the presence of atropine, negative inotropic and chronotropic effects were altered, indicating the presence of cholinergic muscarinic M2 receptor activity and calcium channel blockade activity on cardiac myocytes, which were previously proven on aortic preparation to verapamil (Saqib and Janbaz, 2021).

Hypotensive effect: The experimental findings of Cl.EtOH on aortic preparations and atrium preparation made it a good candidate for possible hypotensive effects on normotensive blood pressure of anesthetized rats. The Cl.EtOH decreases the systolic blood pressure (SBP), diastolic blood pressure (DBP) and means arterial blood pressure (MABP) of the anesthetized rats. These parameters were reduced on pretreatment of atropine (1mg/kg), supporting the speculation of involvement of M_2 receptors located in myocardial tissues and through generalized vasodilation due to non-inverted M_3 receptors on aortic preparations—the calcium channel blockade activity of Cl.EtOH also cannot be ruled out that may play a vital role in the antihypertensive activity of the extract.

Hypertension is produced predominantly by a NO deficiency and oxidative stress in the L-NAME-induced hypertension animal model. The suppression of NO production by L-NAME has some features with human idiopathic hypertension, including ROS-induced cardiovascular abnormalities, inflammation, sympathetic nerve and renin-angiotensin system activation, and cardiovascular remodeling. L-NAME, a nonselective NOS inhibitor, affects both peripheral and central NO production (Aekthammarat et al., 2019). The experimental paradigm of L-NAME--induced hypertension adopted in this study is analogous to that of oxidative stress-induced hypertension produced by a NO deficiency, which are also features of essential hypertension (Kukongviriyapan et al., 2015). The inhibition of NO produces volume-dependent elevation of BP, leads to arterial hypertension and vasoconstriction (Veerappan and Malarvili, 2019). In our results Cl.EtOH decreases L-NAME induce elevated the systolic blood pressure (SBP), diastolic blood pressure (DBP) and means arterial blood pressure (MABP).

ISO induce Myocardial infarction: Myocardial infarction leading cause of abnormalities in heart function and myocardium structure. Isoproterenol administration is widely used in academia to establish myocardial infarctions in experimental animals (Meng et al., 2020; Shao et al., 2013; Zhou et al., 2020). In this study, the cardioprotective effect of Cl.EtOH was studied in ISO to induce chronic myocardial infarctions. The Cl.EtOH restored ISO abnormalities and protected the myocardium tissue. ISO administration caused a significant increase in biometrical indices; heart weight, LHV weight, and other myocardium infarction

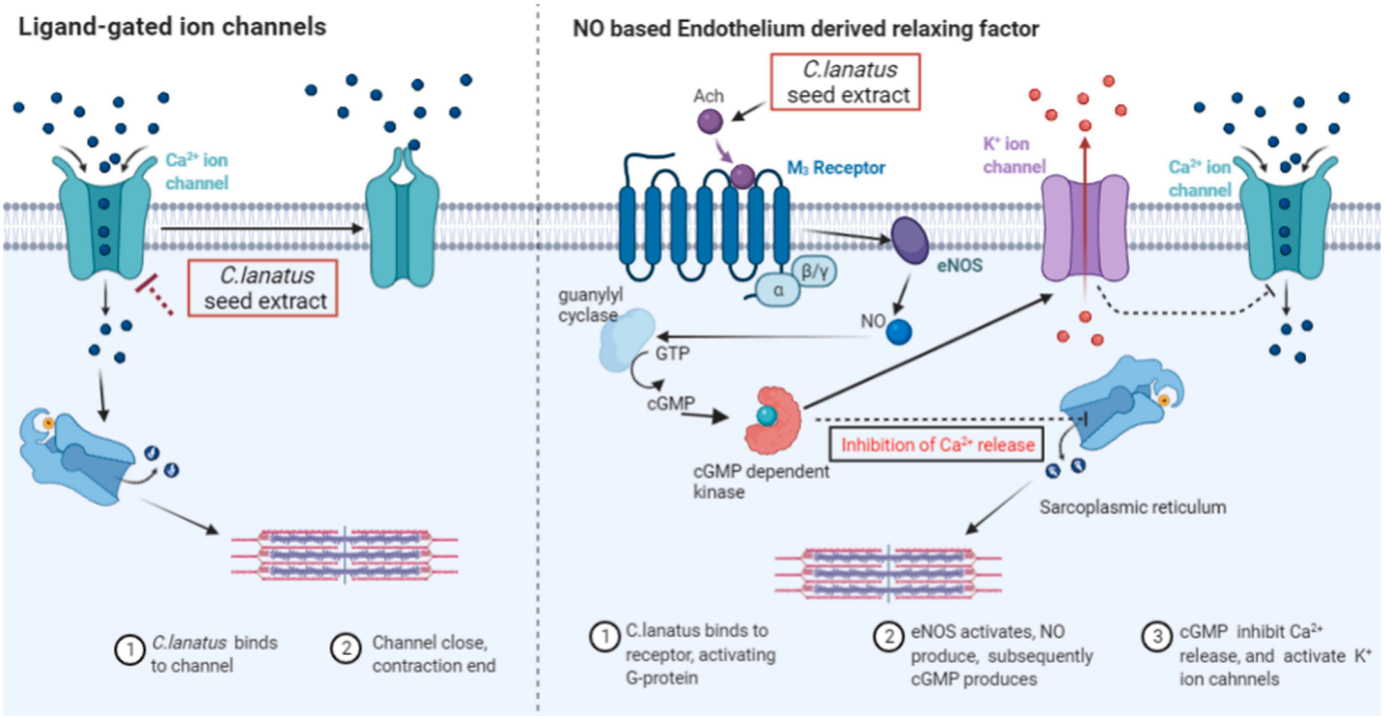

Fig. 11. Mechanistic insight of Cl.EtOH on L type voltage-gated calcium ion channel and NO based endothelium-derived relaxing factor.

parameters, also elevation was observed in serum biochemical parameters levels such as CK, CK-MB, LDH, cTnT, cTnI, BNP, ANP, ALT, AST, ACE and lipid profile. The Cl.EtOH pretreatment and co-administration improved trends in these indices significantly ($p<0.05$) compared to verapamil and carvedilol. The gene expression of myocardial tissues showed Cl.EtOH could attenuate the ISO-induced toxicity effect. It was observed that Cl.EtOH increases the protective role by enhancing eNOS3 mRNA expression, which stimulates vasodilation by the EDRF mechanism (Fig. 11). Besides it, inflammatory proteins IL-6 and MMP-9 and cardiac protein cTnT and ANP increased in ISO group were significantly ($p < 0.05$ vs. ISO group) reverted by Cl.EtOH, verapamil, and carvedilol. Matrix Metallopeptidase 9 (MMP-9) initiates the fibrosis and indicates the degradation of the extracellular matrix (Syed et al., 2016). Its expression was increased in the ISO group due to autophagy and necrosis in myocardial tissues, whereas Cl.EtOH, verapamil, and carvedilol had lower expressions of MMP-9, which may indicate the presence of protection.

It is previously reported that rutin (Filipský et al., 2017; Prince and Karthick, 2007), quercetin (Liu et al., 2012; Punithavathi and Stanely Mainzen Prince, 2011, 2010), naringin (Rajadurai and Mainzen Prince, 2006; Rajadurai and Prince, 2009; Rajadurai and Stanely Mainzen Prince, 2007), kaempferol (Suchal et al., 2016; Zhang et al., 2019), gallic acid (Ryu et al., 2016; Stanely Mainzen Prince et al., 2009), epigallocatechin (Devika and Prince, 2009) protects rats from isoprenaline induce cardiotoxicity. Topal et al., (2018) reported that rutin prevents cisplatin-induced cardiotoxicity and reverses troponin I, CK, CK-MB and TNF-α, levels. Zaafan et al. (2013) reported that quercetin protects the animals from isoprenaline-induced myocardial infarction and reverses the cardiac damage markers, including CK-MB, TNF-α, and cTn-I. Priscilla and Prince, (2009) reported that gallic acid protected the myocardium tissue from isoproterenol-induced oxidative stress and reverted the CK-MB, LDH, AST, ALT, and cTnI. Hackl et al. (2002) reported that quercetin inhibited ACE activity by converting bradykinin and angiotensin, Sanchez et al. (2006) reported that quercetin and isorhamnetin can reduce AnglI-induced endothelial dysfunction.

Metabolomics analysis: The metabolomics analysis of serum and heart samples was conducted to determine the changes of endogenous metabolites among the groups. It was found that Cl.EtOH reverted the ISO-induced abnormalities in potential metabolites biomarkers and their changes associated with the hypotensive effect. The potential biomarkers were part of the following biological pathways; lipid metabolism, oxidative stress, nicotinic and nicotinamide, energy metabolism, and pyruvate metabolism (Fig. 12). The above-mentioned biological pathways are associated with vascular endothelial dysfunction or different etiologies of hypertension (Jiang et al., 2017).

Energy metabolism: Typically, there is a great need for energy in cardiac tissue, but its energy demands extensively increase during myocardial infarctions due to the high utilization of oxygen and adenosine triphosphate (ATP) (Li et al., 2014) and disturbance in myocardial ATP/ADP ratio. Cardiac mitochondria utilize a variety of substrates to

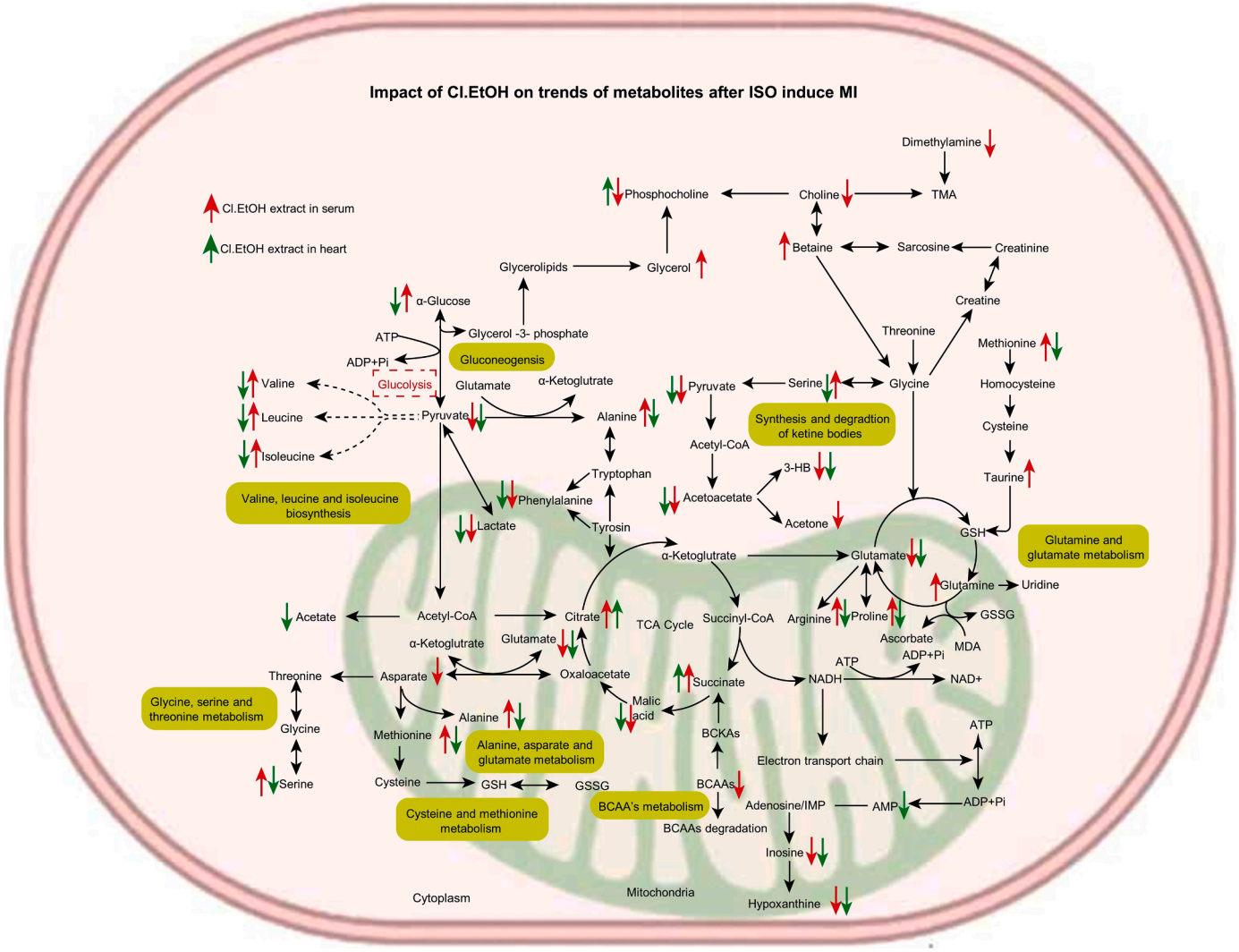

Fig. 12. Effect of Cl.EtOH on trends of metabolites in heart and serum samples after ISO induces MI.

produce ATPs, of which approximately 70 - 80% of ATPs are derived from the oxidation of free fatty acids, and the remaining are derived from carbohydrates, amino acids, and ketone bodies. Previously reported, ISO induces myocardial infraction heart characterized as worse cardiac energy biosynthesis with an accumulation of amino acids and free fatty acids (Luan et al., 2015). Moreover, Cl.EtOH treatment reversed ATP/ADP ratio and increased the ATP availability in the myocardium.

Biosynthesis and degradation of ketone bodies: 3-hydroxybutyrate, acetoacetate, and acetone are members of ketone bodies derived from oxidation of free fatty acids and elevated levels of free fatty acids ISO induced myocardial infraction hearts (Du et al., 2014). The mitochondrial biosynthesis of ketone bodies increased when glucose levels decreased in serum and myocardial tissues during myocardial ischemia. In addition, ISO also significantly ($p < 0.05$ vs. control group) elevated the fumaric acid levels with decreased levels of succinic acid and citric acid compared to the control group. These results indicate abnormalities in Kreb cycle intermediates during myocardial ischemia. The downtrend of serum glucose during myocardial infraction indicated the increased trend of glycolysis to produce ATPs in myocardial tissue (Hunter et al., 2016; Wende et al., 2017).

Pyruvate metabolism: Pyruvate is a terminal metabolite of glycolysis utilized in the Kreb cycle for energy production. Pyruvate is converted into lactate, and the accumulation of lactate leads to increased levels of alanine in myocardial tissue (Wang et al., 2013). The altered glucose levels, pyruvate, lactate, and alanine indicate the impairment in glucose oxidation and increase in glycolysis. These all altered metabolites reflect an altered energy metabolism in ISO myocardial tissue. Cl.EtOH significantly ($p<0.05$ vs. ISO group) reverted the free fatty acids oxidation, ketone bodies (3-hydroxybutyrate, acetoacetate, and acetone), glucose, fumarate, pyruvate, lactate, citrate, succinate, and alanine to improve the energy metabolism, Krebs cycle and glycolysis. Thus, Cl.EtOH increases ATP availability in the myocardium and improves cardiac energy metabolism.

Amino acids metabolism: Certain amino acids degrade into intermediate metabolites to act as cardioprotective substrates in ischemia to increase and supply ATPs. In the metabolomic study, ISO administration altered serum amino acids (aspartate, isoleucine, leucine, glutamate, valine, methionine, glycine, lysine, and alanine) levels samples. This might be due to increased biosynthesis and degradation of amino acids in cardiac tissue to meet the energy requirement. Glutamate, aspartate, glutamine, and branched-chain amino acids (BCAAs, valine, leucine, and isoleucine), used as metabolic substrate tricarboxylic acid (TCA) cycle (Drake et al., 2012). Jiang et al., (2017) found that serum glutamate content was reduced in pyruvate deficiency-induced myocardial infraction and contributed as the intermediate substrate for glycolysis and TCA. Glutamate is a potential indicator of mitochondrial dysfunction and negatively correlates with myocardial infarction. The increased serum glutamate levels facilitate the alternations in the Krebs cycle, amino acids, nucleotide degradation, and ammonia detoxification (Nemutlu et al., 2015). Aquilani et al., (2017) found that in chronic heart failure (CHF) patients, aspartate, glutamate, methionine and cysteine concentrations were decreased as severity of disease increases to meet the metabolic requirements. However, Cl.EtOH regulates these amino acids and is involved in amino acid metabolism to exert a cardioprotective effect.

Branched chain amino acids metabolism and Oxidative stress: Branched chain amino acids (BCAAs) (valine, leucine, and isoleucine), used as alternate substrates to play a significant role in energy production. The myocardium tissues have insufficient capacity than other organs to utilize the BCAAs and produce energy for maintaining heart function (Fu et al., 2018). BCAAs alternation in serum also caused oxidative stress that may cause organ damage (Tso et al., 2014). Branched chain amino acids (BCAAs) alternation in serum also caused oxidative stress that may cause organ damage (Tso et al., 2014). Decrease levels of BCAAs in serum may be due to their accumulation in damaged organs, especially in the heart during ISO-induced MI (Guo et al., 2016). The accumulation of BCAAs in damaged organs leads to energy metabolism disturbance, mitochondrial dysfunction, and mammalian target of rapamycin (mTOR) signaling pathway activation, leading to intensified cardiac dysfunction.

In addition, glutamine, histidine, methionine, and cysteine metabolism are connected to oxidative stress because they are sensitive to all types of reactive oxygen species (ROS) (Bin et al., 2017). Methionine produces glutathione and activates antioxidant enzymes to respond to oxidative stress (Martínez et al., 2017). Bin et al., (2017) reported that methionine protects the myocardium tissue and vasculature from damage by reducing the oxidative stress induced by various oxidants. ISO administration increased the hypoxanthine that upregulates cholesterol and ROS, inducing endothelial dysfunction through oxidative stress and apoptosis (Kim et al., 2017). The nicotinamide ribose, a precursor of nicotinamide (niacinamide) which is component of NADH and NADPH. It regulates oxidative stress by increasing levels of NADPH and antioxidant enzymes. In the present study, ISO administration increases the proline levels; proline is a major component of collagen, and its elevated levels indicate the development of cardiac remodeling (Zimmerli et al., 2008). The results indicate that Cl.EtOH improved the altered BCAAs, glutamine, hypoxanthine, histidine, methionine, cysteine, and nicotinamide levels and reduced oxidative stress. These findings support that Cl.EtOH improves the alternation of amino acid metabolism and upregulates the ammonia fixation and detoxification to protect the heart against myocardial ischemia.

Tryptophan metabolism and production of inflammatory markers: 5-hydroxytryptophan (5-HTP) produced in tryptophan metabolism, and its decarboxylation led to 5-hydroxytryptamine (5-HT, serotonin). Serotonin is a potential inflammatory marker, vasoconstrictor, and neuromodulator. The variation in 5-HTP serum levels modulates the secretion of neurotransmitters such as; epinephrine which has vasoconstriction properties. Through various pathways, nicotinic acid, nicotinamide, and 5-HTP play a crucial role in hypertension and myocardial ischemia. Previous studies report that sphingolipids were involved in etiologies of hypertension (Pörn-Ares et al., 2003). The altered ceramide levels activate the protein kinase then initiate cascade signaling to induce apoptosis. Thereby, eNOS activation was inhibited, oxidative stress was induced in vascular endothelial cells, and production of NO was decreased, both cumulatively causing vascular dysfunction with suppression of endothelium-dependent relaxation of blood vessels. Ceramide also induces arachidonic acid and thromboxane A2 upregulation in the cyclooxygenase pathway. The elevation of both intermediates promotes platelet aggregation and vasoconstriction (Liu et al., 2018). These results support the gene expression and *in vitro* studies that Cl.EtOH improved the cardiac function by eNOS activation and upregulated the endothelium-dependent relaxation (Fig. 11)

Conclusions and future perspectives

In this study, a combination of mechanistically based *in vitro* and *in vivo* experimentation was used to investigate the potential cardioprotective effect of Cl.EtOH. The results suggest that the antihypertensive mechanism of Cl.EtOH may involve the regulation of nitric oxide (NO) based endothelium-derived relaxing factor (EDRF) and is associated with vascular endothelial function. Further, metabolites profiling of serum and heart tissues suggests that Cl.EtOH reversed the ISO-induced myocardial infarction through amino acid metabolism, energy metabolism, and oxidative stress associated with the myocardial infarction. In summary, metabolomic profiling demonstrated mechanistic insight of Cl.EtOH in antihypertensive and cardioprotective activities. This bioinvestigation revealed that Cl.EtOH exhibits significant antihypertensive and cardioprotective activities, which justifies using this plant in the traditional plant medicine of Pakistan and India.

Despite the significant pharmacological potential of *C. lanatus* seeds, more evidence is needed to address some questions from drug discovery

vision. In this regard, a broader look is desirable in the upcoming future to discover novel bioactive compounds and pharmacological aspects for *C. lanatus* seeds. There is also a need to develop some protocols for the quality of seeds used for CVDs.

Author Contributions

F.S., M.W.,A.A.A., and H.T.A. designed the study and performed experiments. F.S., M.W., N.B., M. I., M.M., R.A.M.,A.A.A., O.L.P., and L. M.C. collected data and wrote the manuscript. All authors read carefully and approved the final manuscript. All data were generated in-house, and no paper mill was used. All authors agree to be accountable for all aspects of work, ensuring integrity and accuracy.

Funding bond

This research was partially funded by UEFISCDI grant number PN-IIIP4-

IDPCE-2020-2126 and from the National Research Development Projects to finance excellence (PFE)-14/2022-2024 granted by the Romanian Ministry of Research and Innovation.

Ethical approval bond

Ethical approval was attained from the Ethical Committee of Bahauddin Zakariya University, Multan (EC /04PhDL-S2018) dated 26th March 2018. Researchers agreed using the approved informed consent documented before their enrolment into the study

Data Availability of Statement

The datasets used and/or analyzed of this study are from the corresponding author upon reasonable request.

Declaration of Competing Interest

The authors declare no conflict of interest.

Acknowledgments

The authors want to acknowledge Princess Nourah bint Abdulrahman University Researchers Supporting Project number (PNURSP2022R93), Princess Nourah bint Abdulrahman University, Riyadh, Saudi Arabia.

References

Abu-Reidah, I.M., Arráez-Román, D., Segura-Carretero, A., Fernández-Gutiérrez, A., 2013. Profiling of phenolic and other polar constituents from hydro-methanolic extract of watermelon (Citrullus lanatus) by means of accurate-mass spectrometry (HPLC-ESI-QTOF-MS). Food Res. Int. 51, 354–362. https://doi.org/10.1016/j.foodres.2012.12.033.

Aekthammarat, D., Pannangpetch, P., Tangsucharit, P., 2019. Moringa oleifera leaf extract lowers high blood pressure by alleviating vascular dysfunction and decreasing oxidative stress in L-NAME hypertensive rats. Phytomedicine 54, 9–16. https://doi.org/10.1016/J.PHYMED.2018.10.023.

Ajay, M., Gilani, A.U.H., Mustafa, M.R., 2003. Effects of flavonoids on vascular smooth muscle of the isolated rat thoracic aorta. Life Sci 74, 603–612. https://doi.org/10.1016/j.lfs.2003.06.039.

Aquilani, R., La Rovere, M.T., Corbellini, D., Pasini, E., Verri, M., Barbieri, A., Condino, A.M., Boschi, F., 2017. Plasma amino acid abnormalities in chronic heart failure. Mechanisms, potential risks and targets in human myocardium metabolism. Nutrients 9, 1251. https://doi.org/10.3390/nu9111251.

Bin, P., Huang, R., Zhou, X., 2017. Oxidation resistance of the sulfur amino acids: methionine and cysteine. Biomed Res. Int. https://doi.org/10.1155/2017/9584932, 2017.

Devika, P.T., Prince, P.S.M., 2009. Preventive effect of (-)epigallocatechin gallate on lipids, lipoproteins, and enzymes of lipid metabolism in isoproterenol-induced myocardial infarction in rats. J. Biochem. Mol. Toxicol. 23, 387–393. https://doi.org/10.1002/jbt.20302.

Drake, K.J., Sidorov, V.Y., McGuinness, O.P., Wasserman, D.H., Wikswo, J.P., 2012. Amino acids as metabolic substrates during cardiac ischemia. Exp. Biol. Med. 237, 1369–1378. https://doi.org/10.1258/ebm.2012.012025.

Du, Z., Shen, A., Huang, Y., Su, L., Lai, W., Wang, P., Xie, Zhibing, Xie, Zhiquan, Zeng, Q., Ren, H., Xu, D., 2014. 1H-NMR-based metabolic analysis of human serum reveals novel markers of myocardial energy expenditure in heart failure patients. PLoS One 9, e88102. https://doi.org/10.1371/journal.pone.0088102.

Duke, J.A., 2008. Melon (Cucumis melo L.), in: Duke's Handbook of Medicinal Plants of the Bible. CRC press, New York, pp. 148–151.

Eladwy, R.A., Mantawy, E.M., El-Bakly, W.M., Fares, M., Ramadan, L.A., Azab, S.S., 2018. Mechanistic insights to the cardioprotective effect of blueberry nutraceutical extract in isoprenaline-induced cardiac hypertrophy. Phytomedicine 51, 84–93. https://doi.org/10.1016/j.phymed.2018.10.009.

Elasoru, S.E., Rhana, P., de Oliveira Barreto, T., Naves de Souza, D.L., Menezes-Filho, J.E. R., Souza, D.S., Loes Moreira, M.V., Gomes Campos, M.T., Adedosu, O.T., Roman-Campos, D., Melo, M.M., Cruz, J.S., 2021. Andrographolide protects against isoproterenol-induced myocardial infarction in rats through inhibition of L-type Ca2 + and increase of cardiac transient outward K+ currents. Eur. J. Pharmacol. 906, 174194.

Erhirhie, E., Ekene, N., 2014. Medicinal values on Citrullus lanatus (Watermelon): pharmacological review. Int. J. Res. Pharm. Biomed. Sci. 4, 1305–1312.

Treatment of Ischemic Heart Disease Eschenhagen, T., Brunton, L.L., Hilal-Dandan, R., Knollmann, B.C., 2018. Goodman & Gilman's The Pharmacological Basis of Therapeutics (Eds.). McGraw-Hill, New York, NY, USA.

Filipský, T., Říha, M., Hašková, P., Pilařová, V., Nováková, L., Semecký, V., Vávrová, J., Holečková, M., Palicka, V., Šimůnek, T., Hrdina, R., Mladěnka, P., 2017. Intravenous rutin in rat exacerbates isoprenaline-induced cardiotoxicity likely due to intracellular oxidative stress. Redox Rep 22, 78–90. https://doi.org/10.1080/13510002.2016.1159817.

Fu, J., Chang, L., Harms, A.C., Jia, Z., Wang, H., Wei, C., Qiao, L., Tian, S., Hankemeier, T., Wu, Y., Wang, M., 2018. A metabolomics study of Qiliqiangxin in a rat model of heart failure: a reverse pharmacology approach. Sci. Rep. 8, 1–9. https://doi.org/10.1038/s41598-018-22074-6.

Fusi, F., Saponara, S., Pessina, F., Gorelli, B., Sgaragli, G., 2003. Effects of quercetin and rutin on vascular preparations: a comparison between mechanical and electrophysiological phenomena. Eur. J. Nutr. 42, 10–17. https://doi.org/10.1007/s00394-003-0395-5.

Ghayur, M.N., Khan, H., Gilani, A.H., 2007. Antispasmodic, bronchodilator and vasodilator activities of (+)-catechin, a naturally occurring flavonoid. Arch. Pharm. Res. 30, 970–975. https://doi.org/10.1007/BF02993965.

Gilani, A.H., Khan, A.U., Ghayur, M.N., Ali, S.F., Herzig, J.W., 2006. Antispasmodic effects of Rooibos tea (Aspalathus linearis) is mediated predominantly through K+-channel activation. Basic Clin. Pharmacol. Toxicol. 99, 365–373. https://doi.org/10.1111/j.1742-7843.2006.pto_507.x.

Gilani, A.H., Khan, A.U., Raoof, M., Ghayur, M.N., Siddiqui, B.S., Vohra, W., Begum, S., 2008. Gastrointestinal, selective airways and urinary bladder relaxant effects of Hyoscyamus niger are mediated through dual blockade of muscarinic receptors and Ca2+ channels. Fundam. Clin. Pharmacol. 22, 87–99. https://doi.org/10.1111/j.1472-8206.2007.00561.x.

Gill, N.S., Sood, S., Muthuraman, A., Bali, M., Sharma, Dev, 2011. Evaluation of antioxidant and anti-ulcerative potential of Citrullus lanatus seed extract in rats. Lat. Am. J. Pharm. 30, 429–434.

Guo, J., Yong, Y., Aa, J., Cao, B., Sun, R., Yu, X., Huang, J., Yang, N., Yan, L., Li, X., Cao, J., Aa, N., Yang, Z., Kong, X., Wang, L., Zhu, X., Ma, X., Guo, Z., Zhou, S., Sun, H., Wang, G., 2016. Compound danshen dripping pills modulate the perturbed energy metabolism in a rat model of acute myocardial ischemia. Sci. Rep. 6, 1–13. https://doi.org/10.1038/srep37919.

Hunter, W.G., Kelly, J.P., McGarrah, R.W., Kraus, W.E., Shah, S.H., 2016. Metabolic dysfunction in heart failure: diagnostic, prognostic, and pathophysiologic insights from metabolomic profiling. Curr. Heart Fail. Rep. 13, 119–131. https://doi.org/10.1007/s11897-016-0289-5.

Iswariya, S., Uma, T.S., 2017. Evaluation of in vitro anti-inflammatory and antimicrobial activity of aqueous and methanolic seed extracts of Citrullus lanatus. Int. J. Pharm. Pharm. Sci. 9 (29) https://doi.org/10.22159/ijpps.2017v9i5.16708.

Jiang, M., Wang, Q., Chen, J., Wang, Y., Fan, G., Zhu, Y., 2017. Comparative metabonomics of Wenxin Keli and Verapamil reveals differential roles of gluconeogenesis and fatty acid β-oxidation in myocardial injury protection. Sci. Rep. 7, 1–12. https://doi.org/10.1038/s41598-017-09547-w.

Kamkaew, N., Scholfield, C.N., Ingkaninan, K., Maneesai, P., Parkington, H.C., Tare, M., Chootip, K., 2011. Bacopa monnieri and its constituents is hypotensive in anaesthetized rats and vasodilator in various artery types. J. Ethnopharmacol. 137, 790–795. https://doi.org/10.1016/j.jep.2011.06.045.

Khare, C.P., 2007. Indian Medicinal Plants, Indian Medicinal Plants. Springer, New York, New York, NY. https://doi.org/10.1007/978-0-387-70638-2.

Kim, Y.J., Ryu, H.M., Choi, J.Y., Cho, J.H., Kim, C.D., Park, S.H., Kim, Y.L., 2017. Hypoxanthine causes endothelial dysfunction through oxidative stress-induced apoptosis. Biochem. Biophys. Res. Commun. 482, 821–827. https://doi.org/10.1016/j.bbrc.2016.11.119.

Koocheki, A., Razavi, S.M.A., Milani, E., Moghadam, T.M., Abedini, M., Alamatiyan, S., Izadkhah, S., 2007. Physical properties of watermelon seed as a function of moisture content and variety. Int. Agrophysics 21, 349–359.

Kuhn, B., Kollman, P.A., 2000. Binding of a diverse set of ligands to avidin and streptavidin: an accurate quantitative prediction of their relative affinities by a combination of molecular mechanics and continuum solvent models. J. Med. Chem. 43, 3786–3791. https://doi.org/10.1021/jm000241h.

Kukongviriyapan, U., Kukongviriyapan, V., Pannangpetch, P., Donpunha, W., Sripui, J., Sae-Eaw, A., Boonla, O., 2015. Mamao pomace extract alleviates hypertension and oxidative stress in nitric oxide deficient rats. Nutr. 2015, Vol. 7 (7), 6179–6194. https://doi.org/10.3390/NU7085275, 6179–6194.

Kumar, S., Jahangir Alam, M., Prabhakar, P., Ahmad, S., Maulik, S.K., Sharma, M., Goswami, S.K., 2017. Proteomic analysis of the protective effects of aqueous bark extract of Terminalia arjuna (Roxb.) on isoproterenol-induced cardiac hypertrophy in rats. J. Ethnopharmacol. 198, 98–108. https://doi.org/10.1016/j.jep.2016.12.050.

Lanuzza, F., Occhiuto, F., Monforte, M.T., Tripodo, M.M., D'Angelo, V., Galati, E.M., 2017. Antioxidant phytochemicals of Opuntia ficus-indica (L.) Mill. cladodes with potential anti-spasmodic activity. Pharmacogn. Mag. 13, S424–S429. https://doi.org/10.4103/pm.pm_495_16.

Lee, K.N., Lu, X., Nguyen, C., Feng, Q., Chidiac, P., 2017. Cardiomyocyte specific overexpression of a 37 amino acid domain of regulator of G protein signalling 2 inhibits cardiac hypertrophy and improves function in response to pressure overload in mice. J. Mol. Cell. Cardiol. 108, 194–202. https://doi.org/10.1016/j.yjmcc.2017.06.007.

Li, F., Xu, Q., Zheng, T., Huang, F., Han, L., 2014. Metabonomic analysis of Allium macrostemon Bunge as a treatment for acute myocardial ischemia in rats. J. Pharm. Biomed. Anal. 88, 225–234. https://doi.org/10.1016/j.jpba.2013.09.002.

Liu, A., Chu, Y.J., Wang, X., Yu, R., Jiang, H., Li, Y., Zhou, H., Gong, L.L., Yang, W.Q., Ju, J., 2018. Serum metabolomics study based on LC-MS and antihypertensive effect of uncaria on spontaneously hypertensive rats. evidence-based complement. Altern. Med. https://doi.org/10.1155/2018/9281946, 2018.

Liu, H., Zhang, L., Lu, S., 2012. Evaluation of antioxidant and immunity activities of quercetin in isoproterenol-treated rats. Molecules 17, 4281–4291. https://doi.org/10.3390/molecules17044281.

Luan, A., Tang, F., Yang, Y., Lu, M., Wang, H., Zhang, Y., 2015. Astragalus polysaccharide attenuates isoproterenol-induced cardiac hypertrophy by regulating TNF-α/PGC-1α signaling mediated energy biosynthesis. Environ. Toxicol. Pharmacol. 39, 1081–1090. https://doi.org/10.1016/j.etap.2015.03.014.

Mabaleha, M.B., Mitei, Y.C., Yeboah, S.O., 2007. A comparative study of the properties of selected melon seed oils as potential candidates for development into commercial edible vegetable oils. JAOCS, J. Am. Oil Chem. Soc. 84, 31–36. https://doi.org/10.1007/s11746-006-1003-7.

Martínez, Y., Li, X., Liu, G., Bin, P., Yan, W., Más, D., Valdivié, M., Hu, C.A.A., Ren, W., Yin, Y., 2017. The role of methionine on metabolism, oxidative stress, and diseases. Amino Acids 49, 2091–2098. https://doi.org/10.1007/s00726-017-2494-2.

Massa, N.M.L., Silva, A.S., Toscano, L.T., Silva, J.D., gomes, R., Persuhn, D.C., Gonçalves, M.D.C.R., 2016. Watermelon extract reduces blood pressure but does not change sympathovagal balance in prehypertensive and hypertensive subjects. Blood Press 25, 244–248. https://doi.org/10.3109/08037051.2016.1150561.

Mehmood, M.H., Anila, N., Begum, S., Syed, S.A., Siddiqui, B.S., Gilani, A.H., 2014. Pharmacological basis for the medicinal use of Carissa carandas in constipation and diarrhea. J. Ethnopharmacol. 153, 359–367. https://doi.org/10.1016/j.jep.2014.02.024.

Meng, Y., Du, Z., Li, Y., Gao, P., Song, J., Lu, Y., Tu, P., Jiang, Y., Guo, X., 2020. The synergistic mechanism of total saponins and flavonoids in Notoginseng−Safflower pair against myocardial ischemia uncovered by an integrated metabolomics strategy. Biomed. Pharmacother. 130, 110574 https://doi.org/10.1016/j.biopha.2020.110574.

Nemutlu, E., Zhang, S., Xu, Y.Z., Terzic, A., Zhong, L., Dzeja, P.D., Cha, Y.M., 2015. Cardiac resynchronization therapy induces adaptive metabolic transitions in the metabolomic profile of heart failure. J. Card. Fail. 21, 460–469. https://doi.org/10.1016/j.cardfail.2015.04.005.

Ouassor, I., Aqil, Y., Belmaghraoui, W., El Hajjaji, S., 2020. Characterization of two Moroccan watermelon seeds oil varieties by three different extraction methods. OCL - oilseeds fats. Crop. Lipids 27. https://doi.org/10.1051/ocl/2020010.

Pasupathy, S., Tavella, R., Grover, S., Raman, B., Procter, N.E.K., Du, Y.T., Mahadavan, G., Stafford, I., Heresztyn, T., Holmes, A., Zeitz, C., Arstall, M., Selvanayagam, J., Horowitz, J.D., Beltrame, J.F., 2017. Early use of N-acetylcysteine with nitrate therapy in patients undergoing primary percutaneous coronary intervention for ST-segment-elevation myocardial infarction reduces myocardial infarct size (the NACIAM trial [N-acetylcysteine in acute myocardial inf. Circulation 136, 894–903. https://doi.org/10.1161/CIRCULATIONAHA.117.027575.

Perkins-Veazie, P., Collins, J.K., Clevidence, B., Wu, G., 2007. Watermelons and health, in: acta horticulturae. pp. 121–127. https://doi.org/10.17660/actahortic.2007.731.17.

Pörn-Ares, M.I., Saido, T.C., Andersson, T., Ares, M.P.S., 2003. Oxidized low-density lipoprotein induces calpain-dependent cell death and ubiquitination of caspase 3 in HMEC-1 endothelial cells. Biochem. J. 374, 403–411. https://doi.org/10.1042/BJ20021955.

Prince, P.S.M., Karthick, M., 2007. Preventive effect of rutin on lipids, lipoproteins, and ATPases in normal and isoproterenol-induced myocardial infarction in rats. J. Biochem. Mol. Toxicol. 21, 1–6. https://doi.org/10.1002/jbt.20151.

Priscilla, D.H., Prince, P.S.M., 2009. Cardioprotective effect of gallic acid on cardiac troponin-T, cardiac marker enzymes, lipid peroxidation products and antioxidants in experimentally induced myocardial infarction in Wistar rats. Chem. Biol. Interact. 179, 118–124. https://doi.org/10.1016/j.cbi.2008.12.012.

Punithavathi, V.R., Prince, Stanely Mainzen, 2010. Protective effects of combination of quercetin and α-tocopherol on mitochondrial dysfunction and myocardial infarct size in isoproterenol-treated myocardial infarcted rats: biochemical, transmission electron microscopic, and macroscopic enzyme mapping evi. J. Biochem. Mol. Toxicol. 24, 303–312. https://doi.org/10.1002/jbt.20339.

Qamar, M., Akhtar, S., Ismail, T., Yuan, Y., Ahmad, N., Tawab, A., Ismail, A., Barnard, R. T., Cooper, M.A., Blaskovich, M.A.T., Ziora, Z.M., 2021. Syzygium cumini(L.),Skeels fruit extracts: in vitro and in vivo anti-inflammatory properties. J. Ethnopharmacol. 271, 113805 https://doi.org/10.1016/j.jep.2021.113805.

Rahman, H., Priyanka, P., Lavanya, T., Srilakshni, N., Payili, R.K., 2013. A review on ethnobotany. Phytochemisrty and Pharmacology of. Int. Res. J. Pharm. Appl. Sci 3, 77–81.

Raihana, A.R.N., Marikkar, J.M.N., Amin, I., Shuhaimi, M., 2015. A review on food values of selected tropical fruits seeds. Int. J. Food Prop. 18, 2380–2392. https://doi.org/10.1080/10942912.2014.980946.

Rajadurai, M., Mainzen Prince, P.S., 2006. Preventive effect of naringin on lipids, lipoproteins and lipid metabolic enzymes in isoproterenol-induced myocardial infarction in Wistar rats. J. Biochem. Mol. Toxicol. 20, 191–197. https://doi.org/10.1002/jbt.20136.

Rajadurai, M., Prince, P.S.M., 2009. Naringin ameliorates mitochondrial lipid peroxides, antioxidants and lipids in isoproterenol-induced myocardial infarction in wistar rats. Phyther. Res. 23, 358–362. https://doi.org/10.1002/ptr.2632.

Rajadurai, M., Stanely Mainzen Prince, P., 2007. Preventive effect of naringin on cardiac mitochondrial enzymes during isoproterenol-induced myocardial infarction in rats: a transmission electron microscopic study. J. Biochem. Mol. Toxicol. 21, 354–361. https://doi.org/10.1002/jbt.20203.

Renner, S., Pandey, A., 2013. The Cucurbitaceae of India: accepted names, synonyms, geographic distribution, and information on images and DNA sequences. PhytoKeys 20, 53–118. https://doi.org/10.3897/phytokeys.20.3948.

Rimando, A.M., Perkins-Veazie, P.M., 2005. Determination of citrulline in watermelon rind. J. Chromatogr. A 196–200. https://doi.org/10.1016/j.chroma.2005.05.009, 1078.

Rowan, A.N., 1979. Guide for the Care and Use of Laboratory Animals. J. Med. Primatol. https://doi.org/10.1159/000460187.

Ryu, Y., Jin, L., Kee, H.J., Piao, Z.H., Cho, J.Y., Kim, G.R., Choi, S.Y., Lin, M.Q., Jeong, M. H., 2016. Gallic acid prevents isoproterenol-induced cardiac hypertrophy and fibrosis through regulation of JNK2 signaling and Smad3 binding activity. Sci. Rep. 6, 1–14. https://doi.org/10.1038/srep34790.

Sánchez, M., Galisteo, M., Vera, R., Villar, I.C., Zarzuelo, A., Tamargo, J., Pérez-Vizcaíno, F., Duarte, J., 2006. Quercetin downregulates NADPH oxidase, increases eNOS activity and prevents endothelial dysfunction in spontaneously hypertensive rats. J. Hypertens. 24, 75–84. https://doi.org/10.1097/01.HJH.0000198029.22472.D9.

Saqib, F., Janbaz, K.H., 2021. Ethnopharmacological basis for folkloric claims of Anagallis arvensis Linn. (Scarlet Pimpernel) as prokinetic, spasmolytic and hypotensive in province of Punjab, Pakistan. J. Ethnopharmacol. 267, 113634 https://doi.org/10.1016/j.jep.2020.113634.

Saqib, F., Janbaz, K.H., 2016. Rationalizing ethnopharmacological uses of Alternanthera sessilis: a folk medicinal plant of Pakistan to manage diarrhea, asthma and hypertension. J. Ethnopharmacol. 182, 110–121. https://doi.org/10.1016/j.jep.2016.02.017.

Seraglio, S.K.T., Valese, A.C., Daguer, H., Bergamo, G., Azevedo, M.S., Gonzaga, L.V., Fett, R., Costa, A.C.O., 2016. Development and validation of a LC-ESI-MS/MS method for the determination of phenolic compounds in honeydew honeys with the diluted-and-shoot approach. Food Res. Int. 87, 60–67. https://doi.org/10.1016/j.foodres.2016.06.019.

Shaito, A., Thuan, D.T.B., Phu, H.T., Nguyen, T.H.D., Hasan, H., Halabi, S., Abdelhady, S., Nasrallah, G.K., Eid, A.H., Pintus, G., 2020. Herbal medicine for cardiovascular diseases: efficacy, mechanisms, and safety. Front. Pharmacol. 11 (422) https://doi.org/10.3389/fphar.2020.00422.

Shao, Y., Redfors, B., Mattson-Hultén, L., Scharing Täng, M., Daryoni, E., Said, M., Omerovic, E., 2013. Adenosine prevents isoprenaline-induced cardiac contractile and electrophysiological dysfunction. Eur. J. Pharmacol. 718, 475–483. https://doi.org/10.1016/j.ejphar.2013.07.031.

Sharkey, K.A., MacNaughton, W.K., Brunton, L.L., Hilal-Dandan, R., Knollmann, B.C., 2018. Gastrointestinal Motility and Water Flux, Emesis, and Biliary and Pancreatic Disease. McGraw-Hill, New York, NY, USA, pp. 921–944. Goodman & Gilman's The Pharmacological Basis of Therapeutics.

Siddiqui, W.A., Shahzad, M., Shabbir, A., Ahmad, A., 2018. Evaluation of anti-urolithiatic and diuretic activities of watermelon (Citrullus lanatus) using in vivo and in vitro experiments. Biomed. Pharmacother. 97, 1212–1221. https://doi.org/10.1016/j.biopha.2017.10.162.

Sirous, H., Chemi, G., Campiani, G., Brogi, S., 2019. An integrated in silico screening strategy for identifying promising disruptors of p53-MDM2 interaction. Comput. Biol. Chem. 83 https://doi.org/10.1016/j.compbiolchem.2019.107105.

Suchal, K., Malik, S., Gamad, N., Malhotra, R.K., Goyal, S.N., Bhatia, J., Arya, D.S., 2016. Kampeferol protects against oxidative stress and apoptotic damage in experimental model of isoproterenol-induced cardiac toxicity in rats. Phytomedicine 23, 1401–1408. https://doi.org/10.1016/j.phymed.2016.07.015.

Sun, L., Liu, J., Sun, M., Lin, L., Miao, L., Ge, Z., Yang, B., 2017. Comprehensive metabonomic analysis of heart tissue from isoproterenol-induced myocardial infarction rat based on reversed-phase and hydrophilic interaction chromatography coupled to mass spectrometry. J. Sep. Sci. 40, 2198–2206. https://doi.org/10.1002/jssc.201601013.

Syed, A.A., Lahiri, S., Mohan, D., Valicherla, G.R., Gupta, A.P., Kumar, S., Maurya, R., Bora, H.K., Hanif, K., Gayen, J.R., 2016. Cardioprotective effect of ulmus wallichiana planchon in β-adrenergic agonist induced cardiac hypertrophy. Front. Pharmacol. 7, 1–11. https://doi.org/10.3389/fphar.2016.00510.

Syed, M., Khan, M.N., Khadim, A., Shadab, H., Perveen, A., El-Seedi, H.R., Musharraf, S. G., 2021. Chemical fingerprinting of three Anemone species and an adulteration study to detect cross mixing of medicinal plants by HPLC-HR-ESI-MS/MS method. J. King Saud Univ. - Sci. 33, 101461 https://doi.org/10.1016/j.jksus.2021.101461.

Taiwo, A., Agbotoba, M., Oyedepo, J., Shobo, O., Oluwadare, I., Olawunmi, M., 2009. Effects of drying methods on properties of watermelon (Citrullus lanatus) seed oil. African J. Food, Agric. Nutr. Dev. 8 https://doi.org/10.4314/ajfand.v8i4.19208.

Topal, İ., Bilgin, A.Ö., Çimen, F.K., Kurt, N., Süleyman, Z., Bilgin, Y., Özçiçek, A., Altuner, D., 2018. The effect of rutin on cisplatin-induced oxidative cardiac damage in rats. Anatol. J. Cardiol. 20, 136–142. https://doi.org/10.14744/AnatolJCardiol.2018.32708.

Touyz, R.M., Alves-Lopes, R., Rios, F.J., Camargo, L.L., Anagnostopoulou, A., Arner, A., Montezano, A.C., 2018. Vascular smooth muscle contraction in hypertension. Cardiovasc. Res. 114, 529–539. https://doi.org/10.1093/cvr/cvy023.

Tso, S.C., Gui, W.J., Wu, C.Y., Chuang, J.L., Qi, X., Skvorak, K.J., Dorko, K., Wallace, A. L., Morlock, L.K., Lee, B.H., Hutson, S.M., Strom, S.C., Williams, N.S., Tambar, U.K., Wynn, R.M., Chuang, D.T., 2014. Benzothiophene carboxylate derivatives as novel allosteric inhibitors of branched-chain α-ketoacid dehydrogenase kinase. J. Biol. Chem. 289, 20583–20593. https://doi.org/10.1074/jbc.M114.569251.

Veerappan, R., Malarvili, T., 2019. Chrysin pretreatment improves angiotensin system, cGMP concentration in L-NAME induced hypertensive rats. Indian J. Clin. Biochem. 34, 288–295. https://doi.org/10.1007/S12291-018-0761-Y/FIGURES/5.

Wahid, M., Saqib, F., Ahmedah, H.T., Gavris, C.M., De Feo, V., Hogea, M., Moga, M., Chicea, R., 2021. Cucumis sativus L. seeds ameliorate muscular spasm-induced gastrointestinal and respiratory disorders by simultaneously inhibiting calcium mediated signaling pathway. Pharmaceuticals 14, 1197. https://doi.org/10.3390/ph14111197.

Wang, J., Li, Z., Chen, J., Zhao, H., Luo, L., Chen, C., Xu, X., Zhang, W., Gao, K., Li, B., Zhang, J., Wang, W., 2013. Metabolomic identification of diagnostic plasma biomarkers in humans with chronic heart failure. Mol. Biosyst. 9, 2618–2626. https://doi.org/10.1039/c3mb70227h.

Wende, A.R., Brahma, M.K., McGinnis, G.R., Young, M.E., 2017. Metabolic origins of heart failure. JACC Basic to Transl. Sci. 2, 297–310. https://doi.org/10.1016/J.JACBTS.2016.11.009.

Wu, G., Chen, L., Gu, Y., Hong, Y., Ma, J., Zheng, N., Zhong, J., Liu, A.J., Sheng, L., Zhang, W., Li, H., 2020. Exploring the mechanism underlying the cardioprotective effect of shexiang baoxin pill on acute myocardial infarction rats by comprehensive metabolomics. J. Ethnopharmacol. 259 https://doi.org/10.1016/j.jep.2020.113001.

Zaafan, M.A., Zaki, H.F., El-Brairy, A.I., Kenawy, S.A., 2013. Protective effects of atorvastatin and quercetin on isoprenaline-induced myocardial infarction in rats. Bull. Fac. Pharmacy, Cairo Univ. 51, 35–41. https://doi.org/10.1016/j.bfopcu.2013.03.001.

Zhang, L., Guo, Z., Wang, Y., Geng, J., Han, S., 2019. The protective effect of kaempferol on heart via the regulation of Nrf2, NF-κβ, and PI3K/Akt/GSK-3β signaling pathways in isoproterenol-induced heart failure in diabetic rats. Drug Dev. Res. 80, 294–309. https://doi.org/10.1002/ddr.21495.

Zhou, Y., Li, M., Song, J., Shi, Y., Qin, X., Gao, Z., Lv, Y., Du, G., 2020. The cardioprotective effects of the new crystal form of puerarin in isoproterenol-induced myocardial ischemia rats based on metabolomics. Sci. Rep. 10, 1–18. https://doi.org/10.1038/s41598-020-74246-y.

Zimmerli, L.U., Schiffer, E., Zürbig, P., Good, D.M., Kellmann, M., Mouls, L., Pitt, A.R., Coon, J.J., Schmieder, R.E., Peter, K.H., Mischak, H., Kolch, W., Delles, C., Dominiczak, A.F., 2008. Urinary proteomic biomarkers in coronary artery disease. Mol. Cell. Proteomics 7, 290–298. https://doi.org/10.1074/mcp.M700394-MCP200.